Characterization of the vertical size distribution, composition and chemical properties of dissolved organic matter in the (ultra)oligotrophic Pacific Ocean through a multi-detection approach

P. Fourrier, Gabriel Dulaquais, C. Guigue, P. Giamarchi, G. Sarthou, H. Whitby, R. Riso

Characterization of the vertical size distribution, composition and chemical properties of dissolved organic matter in the (ultra)oligotrophic Pacific Ocean through a multi-detection approach

P. Fourrier[1], G. Dulaquais[*,1], C. Guigue[2], P. Giamarchi[3], G. Sarthou[1], H. Whitby[4] & R. Riso[1]

[1]Laboratoire des Sciences de l'Environnement Marin CNRS UMR 6539, Institut Universitaire Européen de la Mer, Université de Bretagne Occidentale. Place Nicolas Copernic - 29280 Plouzané, France, [2]Aix-Marseille Univ., Université de Toulon, CNRS, IRD, MIO UM 110, Marseille, France, [3]Laboratoire OPTIMAG, Université de Brest, 6 Av. Victor Le Gorgeu, 29285, Brest Cedex, France, [4]Department of Earth, Ocean and Ecological Sciences, School of Environmental Sciences, University of Liverpool, Liverpool, UK.

*Corresponding author. Email: gabriel.dulaquais@univ-brest.fr.

Abstract

This work presents a multi-analytical approach for the characterization of marine dissolved organic matter (DOM). The determination of marine dissolved organic carbon (DOC) was performed by size exclusion chromatography (SEC) and validated using a certified reference material (CRM) as well as through an intercomparison exercise. Multi-detection SEC, fluorescence and electrochemical methods were used in order to describe the size distribution spectra, the composition and chemical properties of marine DOM, in the (ultra)oligotrophic West Tropical South Pacific Ocean (WTSP). In this work, we defined the state of degradation of DOC in the different size fractions, operationally defined by SEC. We estimated that on average 62% of DOC was of humic nature (0.5 – 10 kDa), of which ~ 9% was able to complex trace elements, such as iron (Fe). Our results tend to support that non-refractory DOC is of high molecular weight (HMW), nitrogen (N)-rich, aliphatic, and has a weak fluorescence quantum yield and an enhanced binding capacity for Fe. The ageing of marine DOM occurring within mesopelagic waters is mainly driven by microbial respiration and alters these chemical properties. Although our results are in agreement with a paradigm describing oceanic DOM biogeochemistry known as the size-reactivity continuum, 3 µmolC L^{-1} of very HMW (> 10 kDa) were still observed in a water mass mainly composed of Pacific Deep Waters. This persistence could be explained by a significant content (5%) of aromatic carbon that may protect HMW DOM from long term biodegradation.

Keywords: Dissolved Organic Matter (DOM), Pacific Ocean, Humic Substances (HS), Size Exclusion Chromatography (SEC).

1. Introduction

Marine dissolved organic matter (DOM) is a large pool of reduced carbon (Mackenzie et al., 1981), representing an inventory of similar magnitude to atmospheric carbon. DOM is a complex mixture of thousands of compounds (Gu et al., 1995; Stedmond et al., 2003), mainly small molecules, with an extraordinary diversity of composition (Zark et al., 2017), that results from both abiotic and biotic processes occurring throughout the ocean interior (Hansell et al., 2009).

The size-reactivity continuum provides a paradigm for describing the oceanic biogeochemistry of DOM (Amon & Benner, 1996; Benner & Amon, 2015). According to this model, the ageing of highly (microbially) bioavailable freshly produced matter of high molecular weight (HMW) induce the production of small, oxidized, nitrogen-depleted compounds that are refractory to heterotrophic respiration. This process is thought to be the main pathway of recalcitrant DOM production, also called the microbial carbon pump (Hach et al., 2020; Jiao et al., 2010). The origin of the recalcitrance of DOM is still debated with on the one hand the dilution hypothesis (Arrieta et al., 2015) and on the other hand the molecular hypothesis (Shen & Benner, 2018) but can also result from a combination of both. The recent work of Shen & Benner (2020) tends to validate the fact that the molecular properties of DOM are the primary control on its microbial utilization in the ocean, highlighting the need to develop quantitative proxies of the chemical properties of DOM.

Quantification of DOM can be assessed by the determination of dissolved organic carbon (DOC) concentrations in order to identify the dominant process affecting the entire DOM pool (production *vs.* degradation) in the global ocean (Hansell et al., 2009). Nevertheless, the DOC concentration does not provide information on the nature of DOM and even less on its composition, therefore oceanic studies often combine DOC distributions to specific (structural characterization, Figure S1) or semi-specific qualitative analyses (inferred classification, Figure S1). Mass spectrometry and nuclear magnetic resonance (NMR) techniques are powerful tools to identify molecular formulae and chemical functions in DOM (Benner, 2003; Hertkorn et al., 2013; Kujawinski, 2011; Kujawinski et al., 2009; Mopper et al., 2007; Ogawa & Tanoue 2003 Osterholz et al., 2021). However, these methods need a solid phase extraction (SPE) step prior to analysis and due to the partial extraction yields of the SPE cartridge. At least a third of bulk DOM is lost during this extraction procedure (Dittmar et al., 2008). Moreover, due to the large seawater volume required, these techniques are not easily

applicable for oceanographic expeditions with restricted water budget, involving a large number of parameters. Therefore it is necessary to operationally classify organic compounds according to optical or chemical properties to study DOM biogeochemistry in the ocean. Optical properties of DOM help to identify biogeochemical processes occuring along the water column, and are used as proxies to study the quality (Coble, 2007; Fichot & Benner, 2011), to trace the origin (Fellman et al., 2010; Osburn et al., 2016), and also as indicators of the biological and (photo)chemical processing (Del Vecchio & Blough, 2002; Helms et al., 2013; Osburn et al., 2016) of DOM. However, optical measurements by themselves do not provide robust information on the composition of DOM and need to be combined with complementary analyses. This is supported by a recent critical review of fluorescent DOM revealing the ubiquitousness of fluorescence spectra that « are not tied to biogeochemical origin, but exist across a wide range of different environments » (Wünsch et al., 2019). Semi-specific methods and size exclusion chromatography (SEC) are alternative approaches making it possible to easily differentiate the classes of DOM according to their size and polarity (Amy & Her, 2004; Baghoth et al., 2008; Cornelissen et al., 2008; Dittmar & Kattner 2003; Dulaquais et al., 2018b; Huber & Frimmel, 1994; Huber et al., 2011). No sample extraction or purification are necessary prior to measurements. Coupled with various detectors (carbon, UV, nitrogen), this type of analysis represents an alternative method to study the biogeochemistry of DOM at large scales (Figure S1).

Progress in SEC combined with multiple-detection approaches has made it possible to operationally separate size fractions of DOM, to quantify their DOC content and to describe some of the chemical properties (Amy & Her, 2004, Dulaquais et al., 2018b, Huber et al., 2011). Among others, biopolymers (BP) correspond to a fraction of HMW (> 10 kDa) believed to be mostly constituted of extracellular polymeric substances, such as polysaccharides, proteinaceous material and amino sugars. SEC further permits an operational definition of humic substances (HS) of molecular weight ranging between 0.5 and 10 kDa based on their retention time (e.g. chemical affinity) on a polymethacrylate gel (Huber et al., 2011). Aquatic HS were historically divided into humic acids, which precipitate at pH $\leq$ 1, and fulvic acids soluble at any pH. With SEC, the HS fraction encompasses humic and fulvic acids. According to the literature, HS are believed to derive from phospholipids (Kowalenko & McKercher 1971; Stott & Martin 1990) or produced during the photooxidation of triglycerides and fatty acids (Kieber et al., 1997), but the chemical structure of HS varies depending on their origin (Ertel et al., 1984; Dulaquais et al. 2018a). Recent experiments also

proposed the dimerization of the amino acid tyrosine catalyzed by peroxidase as a possible pathway for HS production (Paerl et al., 2020). Carboxylic-rich alicyclic molecules (CRAM) may represent another significant fraction of operationally defined HS (Hedges et al., 1992). CRAM result from the decomposition of biomolecules derived from phytoplankton, exposed to microbial degradation in the ocean interior (Hertkorn et al., 2006) and could be important iron-binding ligands (Bundy et al., 2015). Part of the HS pool could also be formed during condensation reactions by intermolecular collisions of compounds derived from the degradation of BP (Lehmann and Kleber, 2015; Ogawa & Tanoue, 2003). These condensations occur according to Maillard reactions, between carbohydrates and amino acids or proteins, to form melanoidins (Maillard, 1912). SEC also operationally defines fractions of LMW such as building blocks (BB, 0.3 – 0.5 kDa), LMW acids (< 0.3 kDa, Huber et al., 2011), and LMW neutrals. These LMW fractions are thought to be derived from the fractions in the upper size range (Huber et al., 2011) in agreement with the size reactivity continuum. The BB fraction is supposed to correspond to degraded HS of LMW (Huber et al., 2011), the other two fractions contain, among others, mono-protonic organic acids, mono-oligosaccharides, alcohols, aldehydes, ketones and amino sugars (Amon & Benner, 1994; Huber et al., 2011).

Among the different chemical properties of DOM, the binding capacity for dissolved iron (dFe) is of particular interest. Indeed, it is a key element for marine life and DOM is well-known to enhance dFe solubility by organic complexation (Powell & Donat, 2001; Rue & Bruland, 1995, 1997; van den Berg, 1995; Wu & Luther III, 1995). Several dFe chelators have already been identified including siderophores, exopolysaccharides and humic-like ligands (Gledhill & Buck, 2012). Due to their relative refractory nature, humic-like ligands can be found in the deep ocean (Dulaquais et al., 2018a; Whitby et al., 2020a) and can thereby play an important role in the biogeochemistry of iron (Fe). Electrochemical methods are used to measure the concentrations of the electroactive humic-like substances in marine environments, which are thought to be the fraction of humic-like matter able to complex trace elements, such as Fe (eHS; Dulaquais et al., 2018a, 2020; Sukekava et al., 2018; Whitby & van den Berg, 2015). The quantification of eHS can be a complementary tool to track changes in the binding properties of DOM during its processing, with broader implications for our understanding of the interactions between DOM and trace elements.

In this work we propose a comprehensive view of marine DOM using multiple semi-specific analytical approaches. We present the size fractionation, the aromatic carbon content of DOM and its C:N composition along the entire water column in the oligotrophic gyre of the WTSP. It is commonly assumed that allochtonous DOM is higher in size and more aromatic than that of autochtonous origin. Aromaticity of DOM is one of the main indicators of sources and processes which influence DOM composition (Chen & Hur, 2015; McKnight et al., 2001). C:N elemental ratio of DOM is needed to determine its lability and the state of remineralization of its compounds. N-depleted DOM has been recognized as a typical feature of oligotrophic areas (Kähler & Koeve, 2001), and is further investigated in this manuscript. Samples were collected during the GEOTRACES TONGA (shallow hydroThermal sOurces of trace elemeNts: potential impacts on biological productivity and the bioloGicAl carbon pump, GEOTRACES GPpr14) and US-GP15 expeditions. We also studied the fluorescence properties of DOM and the electroactivity of humic-like substances. The latter analysis provided an estimation of the binding capacity of this humic carbon for dFe.

2. Material and Methods

2.1 Sampling

Samples were collected during two cruises (Figure 1a): TONGA (20° 24.431'S, 166° 35.675'W, GEOTRACES GPpr14 onboard the R/V *L'Atalante* in November 2019) and GEOTRACES US-GP15 (leg 2, 19° 59.99'S, 152° 00.01'W, onboard the R/V *Roger Revelle* in November 2018). During the TONGA cruise, sampling was carried out using a trace metal clean polyurethane powder-coated aluminum frame rosette (TMR) equipped with twenty-four 12 L Teflon-lined GO-FLO bottles (General Oceanics) and attached to a Kevlar® wire. Potential temperature (θ), salinity (S), and dissolved oxygen (O_2), were retrieved from the conductivity–temperature–depth (CTD) sensors (SBE9+) deployed on the TMR. The cleaning protocols of all the sampling equipment followed the guidelines of the GEOTRACES Cookbook (http://www.geotraces.org). After recovery, the TMR was directly transferred into a clean container equipped with a class 100 laminar flow hood. Samples were then taken from the filtrate of particulate samples (collected on acid cleaned polyethersulfone filters, 0.45 μm supor) and collected into acid cleaned and sample-rinsed HDPE 125 mL bottles. Immediately after collection, samples were double bagged and stored at -20°C until analysis in a shorebased laboratory. Samples from the GEOTRACES US-GP15 expedition were collected using the Oceanographic Data Facility's (ODF, Scripps Institution of Oceanography) CTD rosette equipped with twelve 30 L Niskin bottles. Samples were filtered through 0.8/0.45 μm

Acropak 500 filter cartridges and were stored in a -15°C freezer on board. Samples were returned frozen to Stanford University and stored at -20°C thereafter. Aliquots were subsampled in acid cleaned and ultrapure water rinsed 30 mL HDPE bottles at Stanford University within a laminar flow hood (class 100) and sent to LEMAR (Plouzané, France) in a cooler with ice packs (travel duration of 2 days) and finally stored at -20°C until analysis. θ, S, and O_2, were retrieved from the CTD sensors (SBE9+) calibrated with onboard salinity and dissolved oxygen measurements by the ODF group. Details on CTD data access from the TONGA and US-GP15 expeditions are provided in the acknowledgments section.

2.2 Reagents

All aqueous solutions and cleaning procedures used ultrapure water (resistivity > 18.2 MΩ.cm, MilliQ Element, Millipore®). The mobile phase for SEC multi-detection was a phosphate buffer (pH 6.85), prepared by dissolving disodium phosphate (Na_2HPO_4, 6 g, EMSURE®, 99.5%) and monopotassium phosphate (KH_2PO_4, 10 g, EMSURE®, > 99.5%) in ultrapure water (4 L). The acid phase was prepared by adding orthophosphoric acid (H_3PO_4, 16 mL, EMSURE®, 85%) to a solution of potassium persulfate ($K_2S_2O_8$, 2 g, Alfa Aesar, Ward Hill MA, USA, 97%) in ultrapure water (4 L). Calibrations of the organic carbon detector (OCD) and the ultra-violet detector (UVD) were achieved by potassium hydrogen phthalate ($C_8H_5KO_4$, Alfa Aesar, 99.95 – 100.05%). The organic nitrogen detector (OND) calibration was done using urea standard solutions (CH_4N_2O, Merck, Germany, >99.5%). Calibrations were made in artificial seawater. The artificial seawater was prepared by dissolving sodium chloride (NaCl, 6.563 g, ChemaLab NV, Belgium, 99.8%), potassium chloride (KCl, 0.185 g, Merck, Germany, 99.999%), calcium chloride ($CaCl_2$, 0.245 g, Prolabo, France, > 99.5%), magnesium chloride ($MgCl_2$, 1.520 g, Merck, Germany, 99-101%), magnesium sulfate ($MgSO_4$, 1.006 g, Sigma-Aldrich, USA, ≥99%), sodium bicarbonate ($NaHCO_3$, 0.057 g, ChemaLab NV, Belgium, >99.7 %) in ultrapure water (250 mL). Artificial seawater was then UV irradiated for 2 hours in order to remove all traces of organic contaminants. Fulvic (SRFA, 1S101F) and humic acids (SRHA, 1S101H) from the *Suwannee River* used to calibrate the molecular weights (MW) of the HS fraction were provided by the International Humic Substances Society (IHSS). The average molar masses for these fulvic (711 Da) and humic acids (1066 Da) were previously defined by Aiken et al. (1989). Deep seawater reference (DSR) samples were used to validate the DOC measurements and were provided by the *Hansell* research laboratory (batch 19, lot #03-19). Calibration solutions for Total Carbon Analyser (TOC-V) were prepared using $C_8H_5KO_4$ in ultrapure water. A solution of 4 µg L^{-1} quinine sulfate dihydrate (QS, Acros Organics, VWR

Chemical, USA, >99%) in 0.1 M sulfuric acid (H_2SO_4, Fluka®, Sigma-Aldrich, Switzerland, >95%) was used for standardization of fluorescence units. For electrochemical analysis, an acidic solution (hydrochloric acid, HCl, 0.01 M, Suprapur®, >99%) of 1.24 µmol L^{-1} iron (III) was prepared from a stock solution (1 g L^{-1}, VWR, Prolabo, France). The borate buffer (H_3BO_3, 1M, Suprapur®, Merck, Germany, 99.8%) was prepared in 0.4 M ammonium solution (NH_4OH, Ultrapure normatom, VWR Chemical, USA, 20-22%). The potassium bromate solution ($BrKO_3$, 0.3 M, VWR Chemical, USA, ≥ 99.8%) was prepared in ultrapure water. The SRFA (2S101F) standard stock solution (38.2 mg L^{-1}) was prepared in ultrapure water and was then saturated with Fe and equilibrated overnight before use. Exact concentration was determined by SEC analysis.

2.3 Analysis of marine DOM

2.3.1 Size exclusion chromatography (SEC)

The distributions of the different organic compound classes were performed by SEC coupled with an OCD, an OND and a UVD (DOC-Labor®, Karlsruhe, Germany) as previously described by Huber et al. (2011) for natural waters, and adapted for marine waters by Dulaquais et al. (2018b). Repeated analysis of DSR samples (DOC_{DSR} = 43.2 ± 1.7 µmol L^{-1}; n = 5; consensus value of lot #10-18: 43 – 45 µmol L^{-1}) ensures an accurate determination of DOC. The same method and configuration were applied for our samples, but with injection volumes of 2.5 mL. This sample volume was selected to decrease the limits of detection (LOD, Table S1) and to avoid the condensation of DOM observed for injection volumes greater than 3 mL (Dulaquais et al., 2018b). Two chromatographic columns (250 mm × 20 mm, TSK HW-50S, 3000 theoretical plates, Toso, Japan) allows the separation of DOM into five fractions of organic compounds with an optimal resolution (Baghoth et al., 2008). These fractions were described in order of retention as BP (> 10 kDa), HS (0.5 – 10 kDa), BB (0.3 – 0.5 kDa), LMW monoprotic acids and neutrals (< 0.3 kDa, Huber et al., 2011). Their respective hypothetical composition are described in detail in Huber et al. (2011), Dulaquais et al. (2018b) and in Table S1. In this study, C:N ratios were determined in two operationally defined fractions (BP and HS) and the OND was calibrated using urea (instead of nitrate) standards in order to take into account the oxidation yield of organic nitrogen into nitrate. The percentage of aromatic carbon ($\%C_{arom}$) in an operationally defined given fraction was determined according to Riso et al. (2021). It is defined as the spectral absorption coefficient (SAC in m^{-1}) at 254 nm divided by the organic carbon concentration (OC, in gC m^{-3}) of the fraction, and then multiplied by a coefficient of 4.403 (in $\%C_{arom}$ gC m^{-2}). This coefficient was

determined by the correlation between the $\%C_{arom}$ and SAC to [OC] ratio from NMR data determined for a suite of IHSS standards (Riso et al., 2021).

2.3.1 TOC-V analysis

During the TONGA expedition, samples for DOC analysis by TOC-V were taken from a classical rosette equipped with twenty-four 12 L Niskin bottles. The samples were filtered under low vacuum (< 50 mm Hg) through 25 mm glass fiber filters (porosity ~ 0.7 µm, GF/F Whatmann) and transferred into 10 mL glass ampoules. The filtrates were then acidified with 20 µL of H_2SO_4 (95%-98%, Sigma Aldrich), then the ampoules were flame sealed and stored at 4°C until the analysis. DOC concentrations were measured in two replicates on a TOC-V (Shimadzu, Kyoto, Japan) according to Sohrin & Sempéré (2005). The method consist of high temperature (680 °C) platinum (Pt)-catalyzed oxidation coupled to non-dispersive infrared gas detection of carbon dioxide (CO_2). Before injection, the samples were bubbled for 2 min with CO_2-free air to purge inorganic carbon. The accuracy and system blank of the instrument were determined by the analysis of certified water references (batch 19, lot #03-19, *Hansell* Laboratory, Miami, Florida, USA). The nominal precision of the analysis procedure was within 2%.

2.3.3 Fluorescence spectroscopy

Fluorescence analyses were performed on samples from the TONGA expedition. Excitation emission fluorescence matrices (EEM) were generated using a spectrofluorometer Cary Eclipse (Agilent®) equipped with a 150 W xenon excitation lamp. Optical measurements were performed in a 1 cm quartz cell. For each measurement, excitation and emission bandwidths were fixed at 5 nm. EEM were recorded with λ_{Ex} ranging from 200 to 450 nm with an interval of 5 nm between each spectrum, and λ_{Em} ranging from 280 to 510 nm. The scanning speed was set at 1200 nm min^{-1}. The nomenclature defined by Coble (1996) associates peaks B and T to proteinaceous tyrosine-like (λ_{Ex} 225-275 nm, λ_{Em} 300-320 nm) and tryptophan-like (λ_{Ex} 225-275 nm, λ_{Em} 320-380 nm) compounds respectively, and a peak M to marine humic-like substances (λ_{Ex} 310-320 nm, λ_{Em} 380-420 nm) (Coble, 1996; Hudson et al., 2007; Parlanti et al., 2000). To take into account the daily variations of the spectrofluorometer sensitivity, EEM were normalized to the water Raman signal area. A blank correction was carried out by substracting the mean EEM from ultrapure water samples. Fluorescence signals of EEM were converted into quinine sulfate units (QSU; 1 QSU = fluorescence of 1 µg L^{-1} of quinine sulfate in 0.1 M H_2SO_4 at $\lambda_{Ex}/\lambda_{Em}$ = 350/450 nm). This was performed in order to compare our fluorescent measurements with previous studies since QSU is a widely used fluorescence unit. The LOD were defined as three times the standard

deviation of fluorescence intensity for each fluorophore according to the nomenclature defined by Coble (1996), and were 0.9 QSU for peak B (tyrosine-like), 0.7 QSU for peak T (tryptophan-like) and 0.1 QSU for peak M (humic-like). In this work, we mostly focus on three fluorescence intensity indexes. The fluorescence index (FI, λ_{Ex} 370 nm, λ_{Em} 450/500 nm; McKnight et al., 2001), the biological index (BIX, λ_{Ex} 310 nm, λ_{Em} 380/430 nm; Huguet et al., 2009) and the humification index (HIX, λ_{Ex} 255 nm, λ_{Em} 435-480/300-345 nm; Zsolnay et al., 1999) were calculated to trace the origin of marine DOM.

2.3.4 Analysis of electroactive humic-like substances (eHS)

The determination of eHS was performed on samples from the TONGA expedition. Analyses were performed by cathodic stripping voltammetry (CSV) using a polarographic Metrohm 663VA stand connected to a potentiostat/galvanostat (Autolab, Metrohm®,) and to an interface (IME 663, Metrohm®). Data acquisition was done using the NOVA software (version 10.1). The method used in this study was initially developed by Laglera et al. (2007) and adapted by Sukekava et al. (2018). The method is based on the adsorption at pH 8 of an Fe-humic complex at the surface of a mercury drop electrode under oxidative potential (0 V vs Ag/AgCl) and its reduction during linear stripping of potentials (from 0 to -0.8 V vs Ag/AgCl). In the presence of 30 mmol L^{-1} bromate, the reduction of the Fe-humic complex provides a quantitative peak at -0.5 V (vs Ag/AgCl) with an intensity proportional to the concentration. In this study, the pH of samples was set to 8.00 ± 0.05 by the addition of a borate buffer (final concentration 10 mM) and adjusted by small additions of an ammonia solution. All eHS initially present in a sample were Fe-saturated by the addition of 20 nmol L^{-1} Fe in order to determine the total eHS concentration. After equilibration, aliquots (15 mL) of the sample were placed into 3 different teflon® vials (Savillex®); among them two were spiked with a SRFA standard (2S101F; spiked of 50 and 100 µg L^{-1}), and left for overnight equilibration. After equilibration, samples were placed into a Teflon® voltammetric cell and analyzed by linear sweep voltammetry after 180 s of nitrogen (N_2) purge (Alphagaz®, Air liquide) and a 90 s deposition step. Since there is no certified reference material (CRM) of marine HS, all the results are provided in equivalent SRFA per liter. The use of SRFA for the determination of oceanic eHS may induce biais due to possible differences in composition between SRFA batches purchased and to the origin of this material. SRFA come from freshwaters with a high DOM load while the marine environment is characterized by low DOM concentrations. Furthermore freshwater and marine HS have different composition, including binding capacity for iron, as previously shown (Dulaquais et al., 2018a, Esteves et al., 2009; Riso et al., 2021). Efforts should be conducted to develop a program for the

303 production of a marine humic reference material. In absence of an oceanic reference material
304 comparable to the DSR (for DOC) or SAFe (for dFe) samples, the use of this material permits
305 the generation of intercomparable data between labs and studies. Actually this consensus
306 material is easy to purchase and widely use by the scientific community (Bundy et al., 2015;
307 Cabanes et al., 2020; Dulaquais et al., 2018a; Gao & Guéguen 2018; Laglera et al., 2019; Riso
308 et al., 2021; Slagter et al., 2019; Sukekava et al., 2018; Whitby et al., 2020a,b). Errors were
309 calculated based on statistical evaluation of a least squares linear fit to the data. The absence
310 of quantitative signals in ultrapure water ensures no contamination all along the analytical
311 process. Because no blank signal can be detected, the LOD was defined as three times the
312 standard deviation of the lowest concentration measured (23.2 ± 3.0 µg eq-SRFA L^{-1}) and was
313 estimated to be 9 µg eq-SRFA L^{-1}.
314 The four different analyses applied to the respective cruises and stations are presented in
315 Table S2.
316 **3. Results and discussion**
317 **3.1 Hydrography**
318 The hydrography of the WTSP is described in detail by Fumenia et al. (2018), Wagener et al.
319 (2018), Peters et al. (2018) and Villa-Alfageme et al. (2019). In this section we briefly
320 describe the key features encountered. At the sampling locations, salinities ranged from 35.48
321 to 36.15 and temperatures from 23.6 to 27.1°C in the upper 100 m. The oligotrophy of the
322 domain was evidenced by the extremely low surface nutrient concentrations (Cutter et al.,
323 2018; Guieu & Bonnet, 2019) and surface chlorophyll levels derived from satellite data
324 (Figure 1a; MODIS-Aqua MODISA simulations; data from giovanni.gsfc.nasa.gov). At both
325 stations our shallowest sampling depth (25 m) can be considered in the mixed layer and thus
326 representative of surface waters. The thermocline was deep (100–600 m) and was sampled at
327 several depths (Figure 1b). Along the thermocline, different watermasses were identified. The
328 South Pacific Central Waters (SPCW) can be divided by their salinity into the Western
329 (WSPCW) in the upper thermocline and the Eastern (ESPCW) component in the lower
330 thermocline. Modified Equatorial Subsurface Waters (ESSW) may be identified between
331 these two SPCW components. ESSW are known to be poorly oxygenated (Silva et al., 2009)
332 and to have a similar density to SPCW (Sprintall & Tomczak, 1993; Wyrtki, 1967). Thereby
333 the low oxygen concentrations observed in the middle of the thermocline (Figure 1b) were
334 probably induced by an inclusion of ESSW in the SPCW. Below the thermocline, the
335 intermediate waters (600–900 m) were mostly composed of a mix between Subantarctic Mode
336 Waters (SAMW, $26.80 \leq \sigma\theta \leq 27.06$ kg m^{-3}, Hartin et al., 2011) and Antarctic Intermediate

Waters (AAIW, $27.06 \leq \sigma\theta \leq 27.40$ kg m^{-3}, Hartin et al., 2011). Due to the overlap of their potential density, an exact distinction between these two watermasses remains difficult thus they are often considered as a single watermass in the subtropical area (Fumenia et al., 2018). These two watermasses have distinct origins; SAMW are formed by the mix of Antarctic

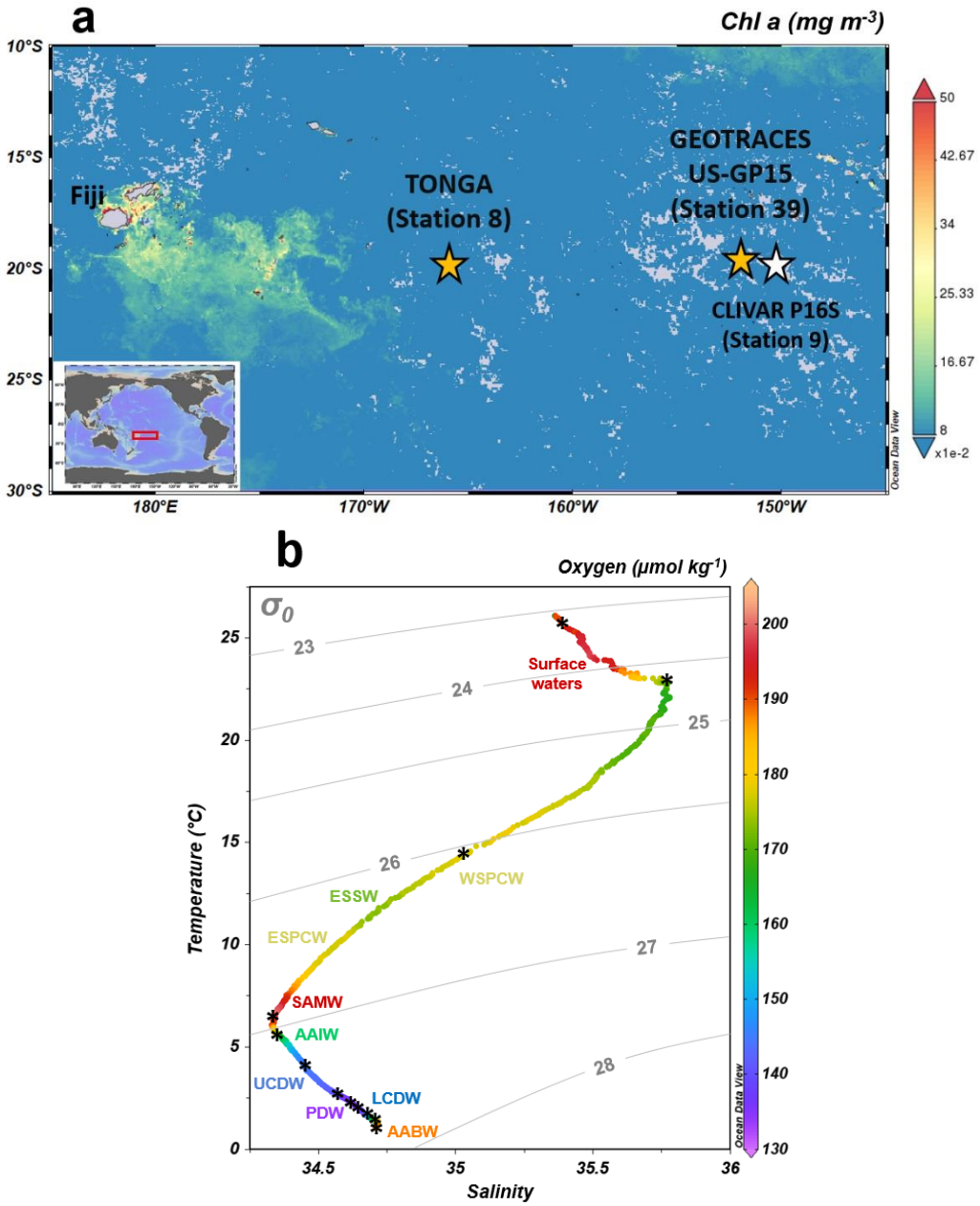

Figure 1. (a) Time averaged map of chlorophyll a (mg m^{-3}; 8-daily 4-km over 2019-11-09 – 2019-12-09) in the Western Tropical South Pacific Ocean (WTSP). Figure generated using Giovanni (giovanni.gsfc.nasa.gov). The two sampled sites of TONGA and GP-15 cruises are indicated (yellow stars), as well as the selected station from CLIVAR P16 for an intercomparison of dissolved organic carbon (DOC) concentrations (white star). **(b)** Temperature/salinity diagram of the study area with the color gradation corresponding to dissolved oxygen (O_2) concentrations (µmol kg^{-1}) at 20° 24.431'S, 166° 35.675'W during the TONGA expedition. Grey lines indicate the isopycnal horizons (on the basis of potential density referenced to a pressure of 0 dbar). Water masses are indicated (see text for abbrevations). Asterisks (*) indicate the samples collected for Size Exclusion Chromatography (SEC) analyses. Figure generated using ODV software.

surface waters with subtropical waters at the subantarctic zone, while AAIW originated from deep convection of the densest Antarctic surface waters at the polar front zone. These distinct locations of downwelling imprint the oxygen signature of these two watermasses, allowing us to distinguish SAMW from AAIW by the higher oxygen content of SAMW (>200 µmol kg^{-1},

Figure 1b) according to McCartney (1979). In the deep sea (>1000 m) the two components (upper and lower) of the circumpolar deep waters (CDW) can be differentiated by their potential density ($\sigma\theta_{UCDW}$ = 27.59, $\sigma\theta_{LCDW}$ = 27.79; Peters et al., 2018; Figure 1b). CDW are the largest water masses of the Southern Ocean and are a mix of AAIW, North Atlantic Deep Waters (NADW) and intermediate water masses from the Pacific Ocean. CDW spread northward in the South Pacific from the Southern Ocean, alongside with the Deep Western Boundary Current (DWBC) of the Pacific Ocean, which flows along the western edge of the Southern basin (Koshlyakov & Tarakanov, 1999). UCDW and LCDW were separated by a layer, centered at 2900 m, mainly composed of PDW ($\sigma\theta_{PDW}$ = 27.77; Peters et al., 2018; Figure 1b). This composite of PDW, UCDW and LCDW is transported northward at this location. In this work, this composite will be considered as the PDW. The most abyssal depths (> 4900 m) were occupied by a composite of LCDW and of Antarctic Bottom Waters (AABW), formed in the Ross Sea. These waters spread northward, driven by Ekman transport and forced by seafloor topography (Tomczak & Godfrey, 2003).

3.2 Vertical distributions of fractions of dissolved organic marine compounds

3.2.1 DOC distribution

The distribution profiles of DOC concentrations (Figure 2) of the four datasets showed a decrease from the surface to the deep waters. With the SEC method used for TONGA samples, the concentrations ranged from 73.4 ± 2.2 µmolC L^{-1} at 25 m depth to 37.4 ± 1.1 µmolC L^{-1} in the old PDW composite at 3400 m, reflecting DOM mineralization in the mesopelagic zone. Deeper, DOC increased again to reach 45.1 ± 1.5 µmolC L^{-1} at the deepest depth (5461 m). These concentrations were higher than the DOC signature of the AABW (40.2 ± 0.7 µmolC L^{-1} in the deep Southern Ocean, Bercovici & Hansell, 2016) located at these depths and could indicate benthic inputs of DOM by diffusion from sediments as previously proposed by Lahajnar et al. (2005) in the deep Atlantic Ocean. To validate DOC measurements, an intercomparison was performed between the DOC concentrations measured by our SEC-OCD system and data acquired using the « classical » TOC-V method. Results are presented in Figure 2 and the two datasets display similar vertical distribution and ranged of concentration for each depth interval. We further compared our measurements to the historic dataset from the P16 CLIVAR expedition at a station located at the same latitude but different longitude (20°S, 150°W) and it showed a good agreement between the three datasets in surface and deep waters. Scatter plot of the paired datasets shows that all the data were close to the 1:1 line (Figure S2) when uncertainties were considered. Good correlations of the

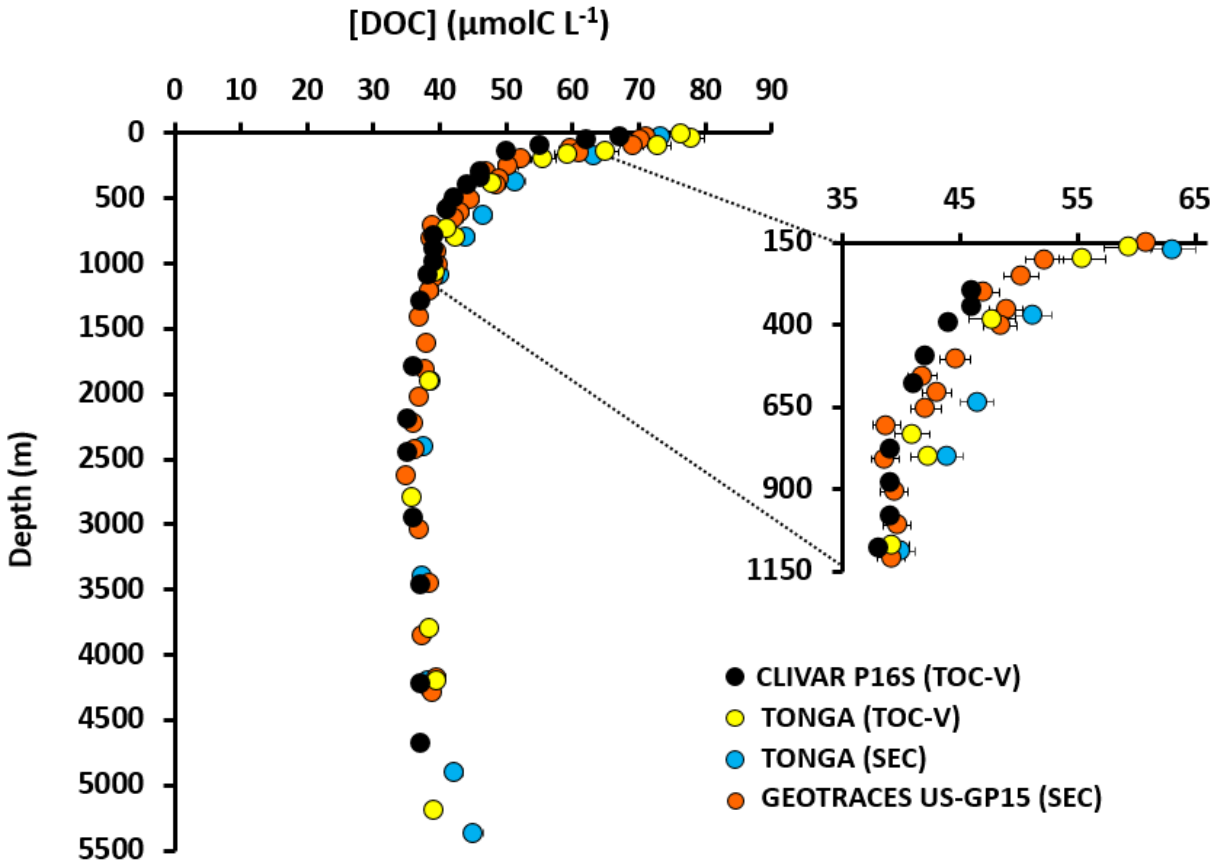

Figure 2. Intercomparison of the DOC concentrations (µmolC L^{-1}) of the TONGA expedition (GEOTRACES GPpr14) at 20° 24.431'S, 166° 35.675'W measured by SEC (blue dots) and TOC-V (yellow dots). Data from the CLIVAR P16 cruise (20°S, 150°W; Swan et al., 2009; dark dots) and from the GEOTRACES US-GP15 cruise (19° 59.99'S, 152° 00.01'W) were also plotted (orange dots).

linear regressions ($R^2 \geq 0.96$) and Spearman coefficients close to 1 (Figure S2), both indicate the strong correlation between DOC concentrations determined by SEC and TOC-V. Together with the accurate determination of DOC in DSR samples, this statistical demonstrate that the SEC-OCD system has an excellent recovery of marine DOC and can be used for accurate quantitative DOC assessment in an open ocean environment. Small discrepancies (see insert Figure 2), higher than uncertainties of the methods, were observed in the mode waters and could be explained by the hydrography. The θ-S diagram shows only small differences in the water composition between P16 and the two stations sampled (Figure S3a) with mode waters being less haline at our locations than during the CLIVAR expedition. This difference of intermediate water composition between ~ 400 and ~ 700 meters depth was however visible by the higher apparent oxygen utilization (AOU) during both the CLIVAR and GP15 expeditions compared to TONGA (Figure S3b). The AOU represents the integrated oxygen consumption by heterotrophic bacteria in the breakdown of organic matter and it is computed as the difference between the oxygen saturation concentration, which depends on thermohaline properties (Weiss, 1970) and the observed oxygen concentration. Thereby the

slightly higher DOC concentration we observed during TONGA (Figure 2) can be linked to a lower DOC mineralization state at these depths than during CLIVAR P16. These observations highlight the imprint of hydrography on DOC distribution.

3.2.2 Size class distribution and composition of DOM

The distribution of the different fractions composing DOM are presented in Figures 3a and in Figure S4 (for TONGA and US-GP15 cruises, respectively). Along the water column, HS had a quasi constant molecular weight (705 ± 20 Da) and was systematically the major fraction of DOC (61.6 ± 2.6 %), with concentrations between 22.2 and 43.2 µmolC L^{-1}. LMW neutral compounds represented the second most abundant fraction, contributing on average to 17.3% of DOC, with an interval of concentration between 6.2 and 11.2 µmolC L^{-1}. The BB fraction accounts for an average of 9.7 ± 1.3 % of DOC throughout the water column, with concentration varying between 3.3 and 6.5 µmolC L^{-1}. BP contributed to 6.7 ± 1.6% (2.0 – 8.0 µmolC L^{-1}) and the fraction containing LMW acids (1.1 – 4.5 µmolC L^{-1}) was the minor component of DOC contributing to only ~ 4.7%.

Within all the different fractions, DOC concentrations decreased from surface to deep waters, but small variations in the partitioning were however observed. For instance, the contribution of the BP and of the LMW acids to DOC decreased from 25 m depth to the 2500-3000 m depth and at the same time the contribution of LMW neutrals increased. These variations can be interpreted as differences in the reactivity of the fractions. HMW compounds seem more labile and consumed more rapidly than small neutral compounds that accumulate with ageing

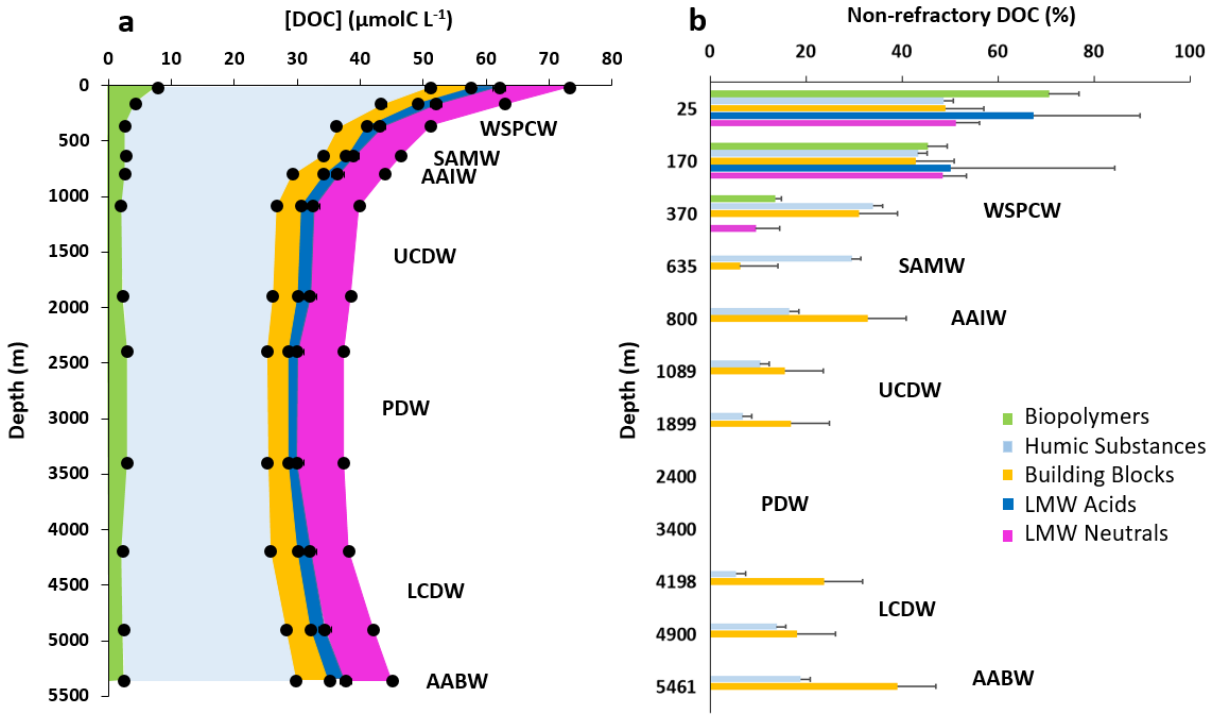

Figure 3. (a) Vertical profiles of the DOC concentrations (µmolC L^{-1}) in the five operational fractions defined by SEC. Non-visible error bars are covered by the symbols. **(b)** Percentage of non-refractory DOC calculated for each fraction (see text for explanation) as a function of depth (m). Depth of water masses are indicated (see text for abbrevations) at 20° 24.431'S, 166° 35.675'W during the TONGA expedition (station 8).

of water masses. These observations are in agreement with the size reactivity continuum described by Benner & Amon (2015) and with the recent study of Zigah et al. (2017) that reports the size partitioning of DOC along the water column from surface to 3500 m depth in the oligotrophic North Pacific Ocean (Station ALOHA). Zigah et al. (2017) estimated a contribution of HMW DOC (defined in their study as > 1kDa) to be between 23 and 35% while LMW hydrophobic compounds (defined in their study as < 1kDa) retained by SPE cartridge accounted for 45-52% of DOC and LMW hydrophilic compounds (non-retained by SPE cartridge) were estimated to account for 22-33% of DOC. Similar to our observations, Zigah et al. (2017) measured HMW DOM throughout the water column and found humic-like substances (called LMW hydrophobic compounds in their study) to be the main fraction composing DOC. The authors further described a distribution of LMW hydrophilic compounds as quasi-homogeneous with a slight enrichment in the surface. The distribution they described is in excellent agreement with those we observed for both LMW acids and neutrals that are LMW hydrophilic compounds. In our study, seawater samples were analyzed without any pre-processing of samples. The excellent agreement of the size-distribution between our study and Zigah et al. (2017) shows that our method allows describing the size distribution of marine DOC with 2.5 mL of sample and without any preliminary filtration and extraction.

DOC refractivity within fractions

At the latitude of sampling, the PDW has an age of over 1000 years (estimated using CLIVAR P16 inorganic $\Delta^{14}C$ at 21°S and ageing equation proposed by Hawco et al., 2018). It has been shown that the organic $\Delta^{14}C$ is even more depleted in the deep Pacific Ocean than the inorganic $\Delta^{14}C$ (Zigah et al., 2017). Thereby DOC can be considered as almost only composed of refractory DOC (RDOC) in this watermass. Due to its refractory nature, the distribution of RDOC is assumed to be conservative (Ogawa & Tanoue, 2003) and can therefore be considered homogeneous throughout the water column. As a result, the DOC concentrations measured for each fraction in the PDW composite can be used to define the contribution of non-RDOC in the different fractions at each depth ([non-RDOC] = [DOC] – $[DOC]_{PDW}$). Despite caveats implied by this assumption (e.g. possible photodegradation of RDOC in the upper euphotic zone, Polimene et al., 2018) it provides a working hypothesis to investigate the chemical properties and reactivity of semi-labile and refractory compounds.

The contribution of non-RDOC for each fraction during the TONGA expedition was calculated for both stations throughout the water column (Figure 3b) and showed a decrease

from surface to the PDW composite depths (2400-3400 m). In surface waters more than 50% of DOC was non-refractory reaching up to 70% for the BP fractions. The decrease of non-RDOC with depth, down to the PDW composite, is observed for all fractions (Figure 3b) and is in agreement with the lability paradigm. However some differences among the fractions were observed with non-RDOC being undetectable in the LMW acids, LMW neutrals and BP fractions below 400 meters depth (Figure 3b) while non-refractory HS, and BB were still depicted. These differences in the non-RDOC distributions are representative of variabilities in the reactivity of the fractions and can be interpreted as the existence of semi-refactory compounds in the BB and HS fractions that were not measured in the other fractions.

Aromatic carbon content of DOM

The aromaticity of DOC was determined for all fractions except for the fraction of LMW neutrals wherein no quantifiable aromatic signal was detected (Figure 4a). In the oligotrophic WTSP, DOM was poorly aromatic with the percentage of aromatic carbon always below 5% in all fractions. In agreement with Medeiros et al. (2015) and Osterholz et al. (2021), our measurements showed surface samples of the Pacific Ocean with extremely low aromatic carbon content and the percentage of aromatic carbon increasing with depth in the upper 1000 m. The higher percentages were observed for the BP and BB fractions in the PDW (2500 – 3500 m). The maximum of aromaticity of BP and BB (~ 5%) is close to those observed for SPE-DOM in the Atlantic Ocean (grey area Figure 4a, 4.57 – 5.13 $\%C_{arom}$; Hertkorn et al., 2013) suggesting that the BP and BB are partly representative of the compounds retained on a SPE cartridge. According to the size-reactivity continuum, occurrence of BP should be limited in old water-masses. However, recent findings suggest that, among others, dissolved black carbon is likely an important fraction of refractory DOM (RDOM) in the ocean (Benner, 2003; Coppola & Druffel, 2016; Dittmar & Koch, 2006; Dittmar & Paeng, 2009; Nakane et al., 2017; Ziolkowski & Druffel, 2010). Black carbon are compounds with

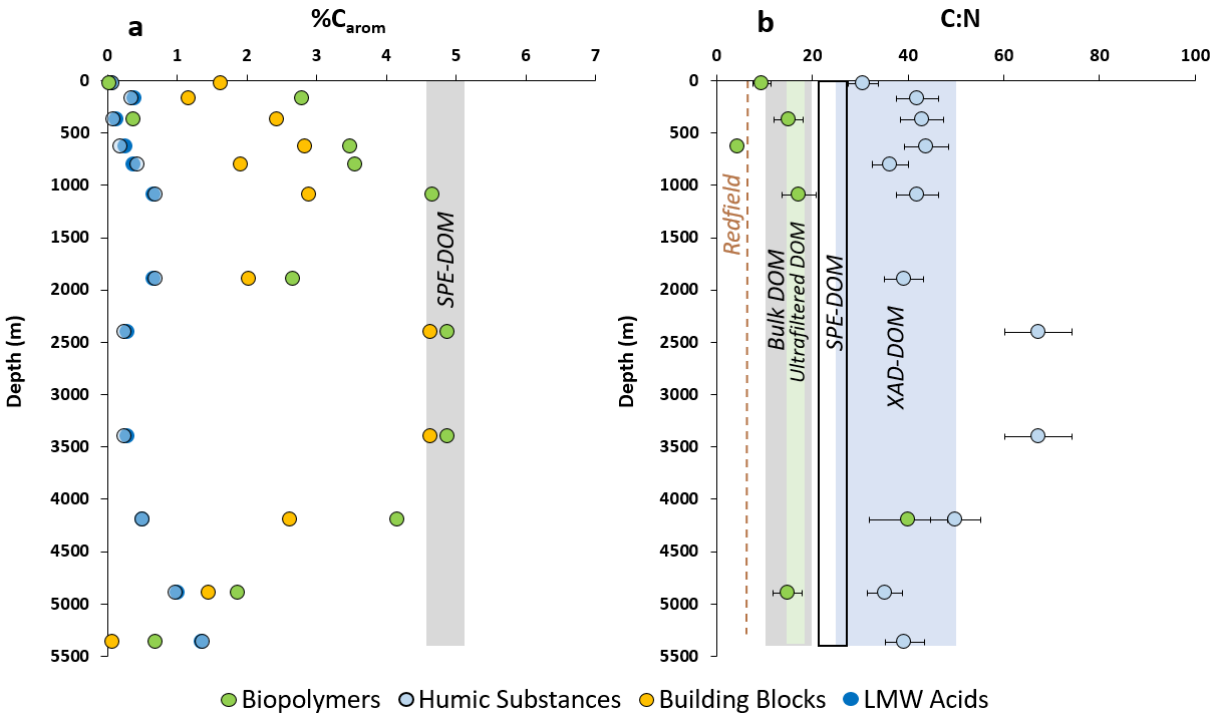

Figure 4. (a) Percentage of aromatic carbon against depth (m) measured in four of the five fractions defined by SEC. Aromatic signal was undetectable in the low molecular weight (LMW) neutral fraction. Range of percentage of aromatic carbon in marine SPE-DOM from the Atlantic Ocean (Hertkorn et al., 2013) is also provided for comparison. **(b)** Elemental C:N ratios measured in the biopolymers (BP) and humic substances (HS) fractions along the water column at 20° 24.431'S, 166° 35.675'W during the TONGA expedition (station 8). Redfield ratio as well as the different ranges of marine C:N ratio in bulk, ultrafiltered, XAD-resin isolated DOM (Hessen & Tranvik, 2013) and SPE-DOM of the Central Pacific Ocean (Green et al., 2014) are provided. Non-visible error bars are covered by the symbols.

condensed rings, ultra-refractory to biodegradation (Dittmar, 2008; Marques et al., 2017; Nakane et al., 2017; Wagner et al., 2018) and can be found under HMW compounds in the deep Pacific Ocean (Ziolkowski & Druffel, 2010). The high percentage of aromatic carbon measured in the PDW for BP and BB possibly indicates the presence of black carbon of both HMW and LMW at these depths, explaining the persistence of these fractions in the PDW. Deeper, $\%C_{arom}$ decreases in the water masses containing non-RDOC. This feature suggests that the $\%C_{arom}$ increases with the refractory nature of BP and BB. The aromaticities of HS and LMW acids were significantly lower (0.1 to 1.4% of C_{arom}) than those of BP and BB. The extremely low aromatic carbon content of HS contrast with those measured in humic standards (e.g. $SRFA_{2S101F}$ = 22%C_{arom}, IHSS) and in estuarine humic-like substances (Riso et al., 2021) confirming the difference in the chemical composition of terrestrial and marine HS, the latter being known to have extremely low aromaticity (Harvey et al., 1983; Hertkorn et al., 2006; Malcolm, 1990; Repeta et al., 2002). The near-zero values in aromatic content measured at the surface may result from a production of HS mainly aliphatics together with the UV-oxidation of their aromaticity (Corin et al., 1996; Miranda et al., 2020; Zhao et al.,

2020). Then, the increase of $\%C_{arom}$ in the mesopelagic layer down to 2000 m can be interpreted as a condensation of HS during their biodegradation/transformation by bacteria into semi-refractory DOM. In the PDW, the $\%C_{arom}$ of refractory HS was extremely low (0.25%) and contrasted with the BP and BB fractions. This result possibly indicates that long term biogeochemical processes occuring in the abyssal waters alter the aromaticity of HS (aromatic rings and conjugated double bounds) formed in the mesopelagic layer. The percentage of C_{arom} increased again in the younger water masses (LCDW, AABW) found deeper and close to sediments in line with the occurrence of HS with an advanced state of biodegradation that are a mix of semi-refractory and refractory HS (Figure 3b).

BB are considered as by-products of HS since ultrasonification experiments were conducted on this DOC fraction (Huber et al., 2011). However, significant correlations were observed between the $\%C_{arom}$ of BP and BB ($R^2 = 0.5408$; $r_s = 0.85$) and between HS and LMW acids ($R^2 = 0.9895$; $r_s = 0.92$). For the two datasets tested, *Spearman* coefficients r_s close to 1, further suggesting links existing between these fractions. According to the size-reactivity continuum, small compounds are produced from the degradation of larger compounds. Based on the aromatic signature we measured in the fraction, we propose to reconsider the BB as by-products of the degradation of BP and LMW acids to be generated during the degradation of HS. This simple definition could then be used to monitor the state of DOM degradation by following a simple ratio (BP/BB or HS/LMW acids) at large scales. Distribution of the BP/BB ratio (data not shown) evidenced a global decrease from surface to deep in agreement with a gradual increase in the state of degradation of DOM with ageing of watermasses. Based on our measurements, we suggest to no longer consider BB as byproducts of HS, as initially postulated in Gaid (2011), in open ocean studies. Overall the results of this study lead to similar conclusions to those obtained from the molecular approach of Osterholz et al. (2021) that shows a significant increase of the DOM degradation index from surface waters to the deep layers of the south east oligothrophic Pacific Ocean.

C:N elemental ratios in BP and HS

N-content of DOM is of interest to investigate the lability of DOM (Vallino et al., 1996). Due to the analytical challenge to measure these extremely low organic nitrogen concentrations studies reporting the C:N ratios of specific DOM compounds in the open ocean are still scarce. In this work we succeed to measure sub-micromolar organic nitrogen concentrations in the HS and BP fractions and present the vertical distribution of their respective C:N ratios (Figure 4b).

During the TONGA expedition, the mean C:N ratio in the HS fraction was relatively homogenous (44.7 ± 4.7; n = 12) with the exception of PDW samples wherein the C:N ratio was significantly higher (67.4 ± 7.1) and can be defined as the C:N ratio of refractory HS. In the shallowest sample (25 m depth) the C:N ratio of HS was 30.7 ± 3.2. These values are higher than those measured in SPE DOM of the Pacific Ocean (21.3 – 27.6; Green et al., 2014) and lower than those of the *Suwannee River* IHSS standards (e.g. C:N $SRFA_{2S101F}$ = 91.1; C:N $SRHA_{1S101H}$ = 51.5; IHSS) except for the PDW samples. These values are however in agreement to the C:N ratios determined in marine HS isolated using XAD resins (Druffel et al., 1992; Hedges et al., 1992; Lara et al., 1993) including those measured in the open Pacific Ocean (e.g. 32 – 43, Meyers-Schulte & Hedges, 1986; Hedges et al., 1992). Vertical variations of the C:N values we measured indicate differences in the bioavailability of nitrogen and carbon in humic matter. Occurrence of a low C:N ratio (30.7 ± 3.2) at 25 m depth suggests two pools of humic-like substances, the refractory HS (high C:N) depleted in nitrogen and the non-refractory HS (low C:N), a N-rich organic matter. Non-refractory HS are possibly generated during the surface degradation of marine phytoplankton (N-rich) and its processing by marine bacteria (cellular lysis, microbial transformation). Culture experiments showing the formation of humic-like compounds (identified by absorbance and fluorescence) during phytoplankton degradation by bacteria (Osburn et al., 2019) support this pathway of production. The increase of the C:N elemental ratio with depth indicate a non-redfieldian mineralization of HS and suggests a preferential remineralization of organic nitrogen compared to organic carbon.

In the BP fraction, C:N ratios (Figure 4b) varied between 4.5 (at 635 m) to 40.1 (at 4198 m). In the upper 1000 meters depth, the C:N ratios of this fraction fall into the range reported for ultrafiltered DOM (HMW DOM; 15-18; Hessen & Tranvik, 2013) which is the definition of BP. In this fraction no organic nitrogen signal can be detected between 1899 m and 3400 m, indicating that refractory HMW compounds are totally nitrogen depleted in the deep Pacific Ocean. BP are mainly composed of proteinaceous material in surface water and with only 30% of refractory matter. They can be considered freshly produced and very labile. Absence of a nitrogen signal in the deep ocean evidences a total utilization of the nitrogen content in the BP fraction during remineralization. Here again a preferential mineralization of nitrogen compared to carbon is observed, suggesting that BP is an important nitrogen reservoir for heterotrophic bacteria. Similar non-redfieldian stoichiometry during DOM mineralization has already been proposed and modeled (Aminot & Kérouel, 2004; Letscher & Moore, 2015; Osterholz et al., 2021). Our results confirm the preferential mineralization of nitrogen

compared to carbon and suggest that the lability of organic compounds may be tightly linked to their nitrogen content.

3.3 Fluorescent properties of DOM

Fluorescence intensities of three different fluorophores (peaks T, B and M) were measured along the water column. Measured values largely exceed LOD (see Figure S5), the intensities and the vertical distributions we report are in agreement with existing data for marine waters (Tedetti et al., 2011; Yamashita & Tanoue, 2004). Despite the flaws of fluorescence methods, such as the quenching effect (Chen et al., 2013; Poulin et al., 2014; Yamashita & Jaffé, 2008) and the ubiquity of some fluorophores (Wünsch et al., 2019), it can provide useful information on the transformation of DOM in the environment. In this section, we focus on the vertical distributions of fluorescent indices during the TONGA expedition. Three fluorescent indices (FI, BIX and HIX) were measured along the water column to further characterize DOM (Figure 5). These indices were determined based on the works of McKnight et al. (2001), Huguet et al. (2009) and Zsolnay et al. (1999) respectively. FI is commonly used to track the DOM sources, in particular to distinguish microbially-derived (FI > 1.9) and terrestrially-derived DOM (FI < 1.4) in marine waters. Along the water column FI ranged between 0.2 (5461 m) and 7.0 (370 m). At 25 m and close to the bottom, values were below 1.4, indicating the existence of a DOM with a FI comparable to terrestrial material. A low FI close to the sediments may be conceivable however it is unusual in surface waters far away from terrestrial influence and without terrestrial eolian inputs (monitored using air mass backward trajectories from the ensemble Hysplit model, ready.noaa.gov/HYSPLIT.php). In absence of a clear terrestrial influence we relate the low surface FI value to photobleaching. Photobleaching of FI is not systematic for freshwater DOM (Helms et al., 2014) and, to our knowledge, has not been reported in marine environment. If proven to be true, the photobleaching of FI in marine waters have implications for the use of the low FI as a proxy of terrestrial DOM. A low FI in marine environment should not be systematically assimilated to a terrestrial influence, especially in environment receiving high solar irradiation (e.g. subtropical domains). Below the euphotic layer, the FI sharply increased in the mesopelagic waters to reach 7.0 ± 0.4 and remained high down to 1000 meters depth. These high FI values suggest the production of microbially-derived DOM (Burdige et al., 2004; Coble 1996) in this layer (100-1000 m). This increase of FI could be related to the mineralization of a sinking biomass, produced in the surface, as well as to a microbial transformation of the labile DOM derived from biomass degradation. The lower values of the FI in the deep sea (Figure 5a)

suggest little to no production of microbial DOM below 1089 m (with the exception of FI = 2.9 ± 0.1 at 3400 m).

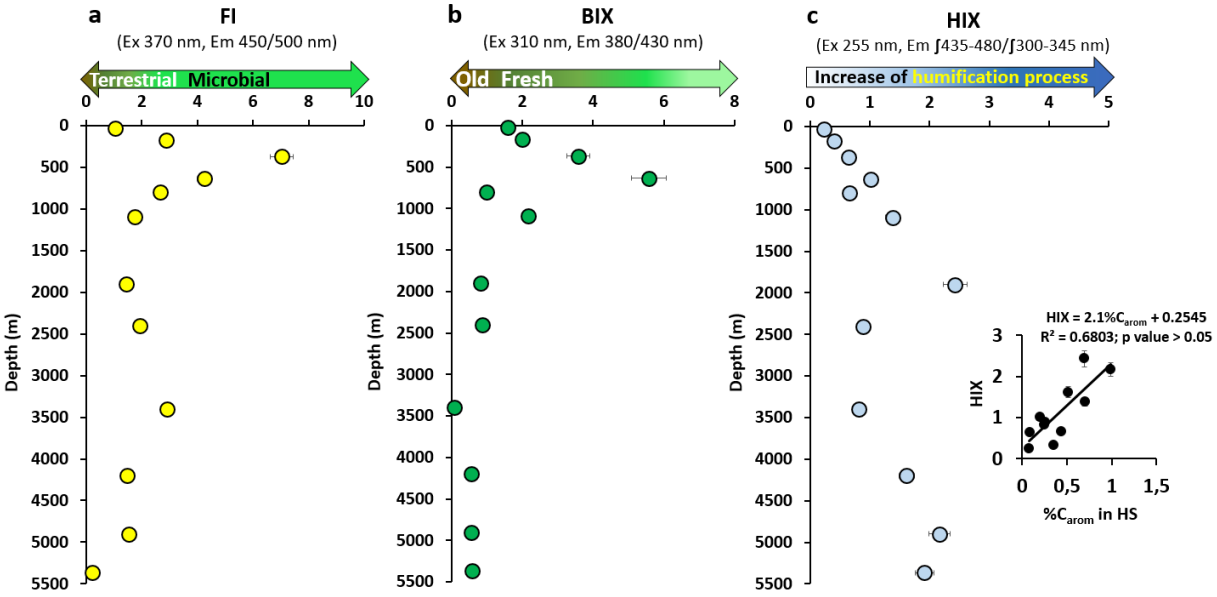

Figure 5. Vertical profiles of **(a)** fluorescence index (FI); **(b)** biological index (BIX); **(c)** humification index (HIX) at 20° 24.431'S, 166° 35.675'W during the TONGA expedition (station 8). Nomenclature of index follows those defined by McKnight et al., (2001), Huguet et al., (2009) and Zsolnay et al., (1999) respectively. Insert in **(c)** shows the significant correlation (*p* value = 0.002) recorded between the HIX and the percentage of aromatic carbon in the SEC HS fraction (Figure 4a).

The distribution of BIX (Figure 5b) corroborates FI results and provides an estimate of the freshness of DOM compounds. A BIX higher than 1 is representative of relatively young DOM, produced *in situ*, while a BIX below 0.6 indicates the occurrence of older DOM that may suffer from long term processing (e.g. biodegradation, photodegradation, Huguet et al., 2009). The BIX values measured ($0.02 \leq BIX \leq 5.57$) show that DOM can be considered relatively young from the surface down to 1089 m, confirming the production of DOM in this zone. Abyssal waters had BIX < 1 implying the presence of old DOM in the deep sea, in agreement with the high proportion of RDOM (Figure 3b). Combining FI and BIX results as well as the distribution of non-RDOM allowed us to better characterize the dynamics of DOM processing in the mesopelagic waters. In the upper 600 meters, the degradation of sinking biomass by heterotrophic bacteria produced young HS and BP that were non-refractory and N-rich (Figure 3b). These new compounds represented a substantial percentage of DOM. Deeper, BB and LMW acids were newly produced (increase of non-refractory percentage) as a result of the degradation of the non-refractory BP and HS (Figure 3b). This production of BB and LMW acids was observed in the zone (~ 300-700 m) where FI and BIX were maximum. These observations suggest that BB and LMW acids could be proxies of microbial mineralization products.

HIX is another indirect proxy of the chemical properties of DOM, highlighting the degree of humification of organic matter in aquatic environments (Miranda et al., 2018; Zsolnay, 2003). HIX ranged from 0.24 at 25 m to 2.4 at 1899 m depth (Figure 3c). HIX increased from the shallow waters (0.24 ± 0.02) to the deep sea (HIX > 1) with the exception of the PDW wherein relatively low HIX were measured (HIX = 0.88 ± 0.02). Throughout the water column, HIX were on average much lower than values measured for vascular plants (1.15 – 4.33; Ohno et al., 2007), soils (> 8; Kalbitz et al., 2003), terrestrial aquatic humics from the IHSS (20 – 50; Birdwell & Engel, 2010) and estuarine and coastal DOM samples (~ 4 – 16; Huguet et al., 2009). HIX measured in this work were in agreement with those of Chen et al. (2017) in the Arctic sector of the Pacific Ocean and we propose to define that a HIX below ~ 2.5 indicates a DOM of primarily marine origin. The very low HIX at 25 m depth (Figure 5c) is in agreement with previous observations in the oligotrophic waters of the Indian Ocean (0.9 ± 0.4; Tedetti et al., 2011) and in the Mediterranean Sea (0.90 ± 0.35 at 5 m depth; Para et al., 2010). Low HIX in the surface can be related to the phenomenon of photobleaching. Solar irradiance is known to strongly decrease HIX of DOM in freshwater samples (Helms et al., 2014; Para et al., 2010) and a similar process was suggested for Mediterranean sea surface samples (Para et al., 2010). The longterm exposition of marine DOM to solar irradiance and subsequent fluorescence extinction is the most likely process explaining the low HIX we measured in the oligotrophic Pacific surface ocean. The increasing values of HIX with depth across the mesopelagic layer (Figure 5c) suggest a humification of DOM. We relate it to the transformation of fresh organic matter into an oxidized fluorescent DOM by the microbial loop. A similar process was previously invoked to explain the increase of the humic-like fluorescence of DOM in this oceanic basin (Yamashita & Tanoue, 2008; 2009; Yamashita et al., 2010). According to Paerl et al. (2020), the production of humic-like fluorescent compounds can also be related to a dimerization of tyrosine catalyzed by peroxidase enzymes on a short timescale (~hours). During microbial degradation of sinking biomass, this amino-acid may be released and dimerized by ambient microbial peroxidase therefore increasing humic-like fluorescence in the mesopelagic waters. HIX often correlates with the aromaticity of organic matter, as observed in estuarine (Huguet et al., 2009) and soil (Segnini et al., 2010) samples as well as for humic reference materials (Ateia et al., 2017). The low HIX values we determined indicate that DOM was poorly aromatic (Birdwell & Engel, 2010) in agreement with the low aromatic carbon content we measured in the different fractions (Figure 4a). Similar to previous works, we observed a significant correlation ($R^2 = 0.6803$; p value < 0.05)

between HIX and $\%C_{arom}$ in the HS fraction (insert in Figure 5c). This result demonstrates that the HS fraction operationally defined by SEC is well representative of the humic material. Such simultaneous increase of HIX and aromaticity has been observed during microbial degradation experiments of soil organic matter (Kalbitz et al., 2003). Moreover, there is recent evidence that HIX increases during the microbial degradation of phytoplankton biomass (Kinsey et al., 2018), indicating that microbial processing also controls the humification of DOM in marine systems. Low HIX in the older PDW are consistent with the low aromatic carbon content of HS (Figure 5a) further suggesting an alteration of aromaticity with ageing of refractory humic matter. The increase of HIX in the deepest samples (Figure 5c) is likely representative of the mixing between watermasses formed in different areas with DOM content of different ages and thus of different degrees of decomposition. Finally, the concomitant increase of humic-like fluorescence (e.g. peak M, Figure S5 and HIX Figure 5c) and decrease of humic-like carbon evidence a gain of fluorescence quantum yield by the humic material during its microbial processing in the mesopelagic waters. Fluorescence spectroscopy is thereby useful to identify the humification process but not to quantify the fraction of DOC related to humic matter in marine environments.

Our results show that fluorescence data are usable proxies for the study of DOM bioavailability when associated to quantitative DOM data ([DOC] and $\%C_{arom}$ in the isolated fractions). In this work, the use of this combination on field samples confirms experimental observations during heterotrophic bacteria incubations (Zheng et al., 2019). Microbial ageing of a relatively labile DOM, originating from oligotrophic phytoplankton, induces the consumption of a low aromatic DOM with a low humic-like fluorescent signature and its transformation to RDOM displaying a high humic-like fluorescence signature and enriched in aromatic carbon.

3.4 Iron binding properties of oceanic humic substances

We further characterized the chemical properties of HS in the WTSP by determining their electroactivity and thereby their complexing capacity for dFe. The concentrations of eHS ranged from 23.2 to 160.2 µg-eqSRFA L^{-1} (Figure 6a).

These concentrations are in agreement with those reported in other marine environments including the Pacific Ocean (Cabanes et al., 2020; Dulaquais et al., 2018a; Laglera et al., 2019; Whitby et al., 2020a). The vertical distribution of eHS displays the typical profile reported in these previous studies, with a surface enrichment and low concentrations in the deep sea. The surface enrichment can be related to a production of eHS during bacterial

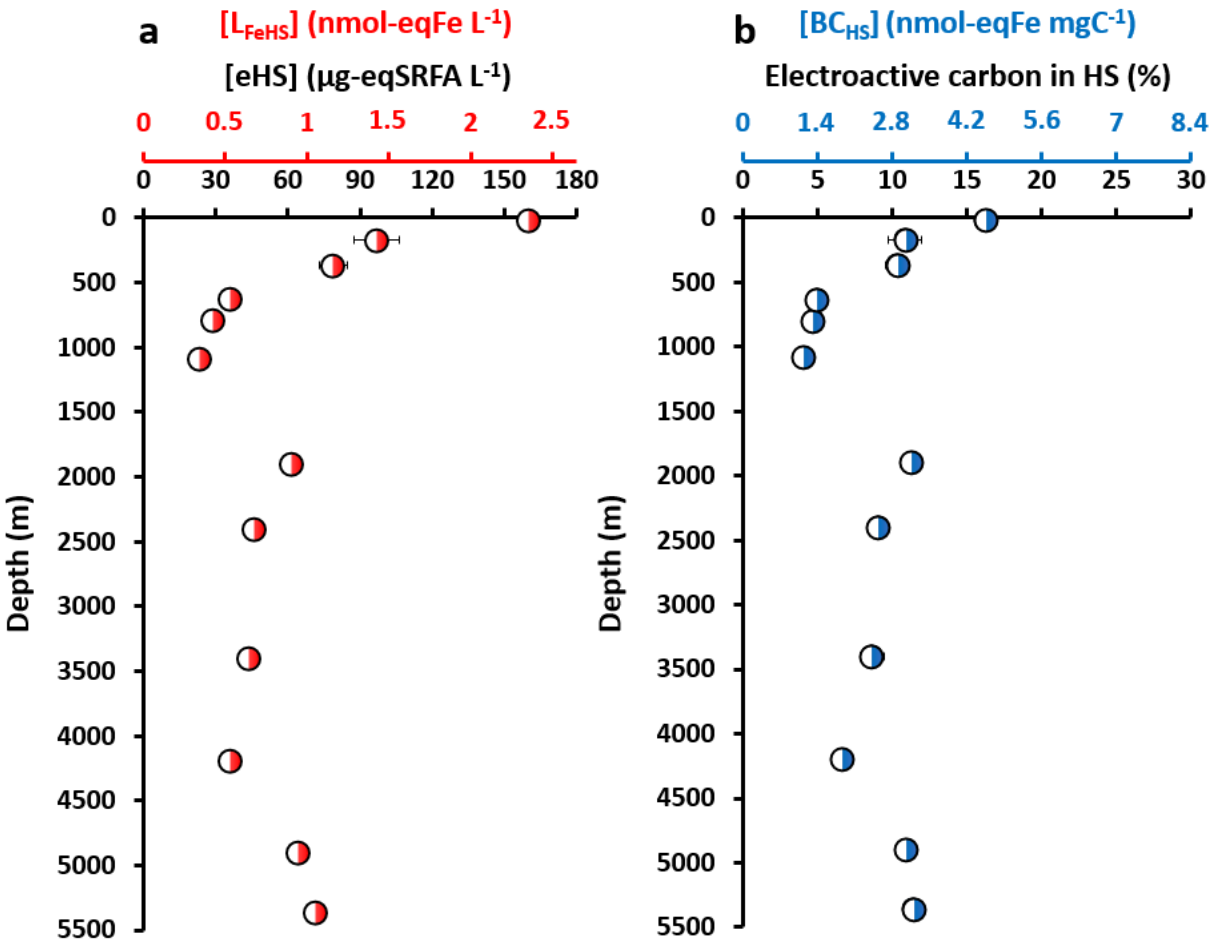

Figure 6. Vertical distributions of the concentrations of **(a)** electroactive humic substances (eHS, expressed in µg-eqSRFA L^{-1}) and humic-type ligands (L_{FeHS}) expressed in nmol-eqFe L^{-1} (calculated following Dulaquais et al., 2018b and Sukekava et al., 2018); **(b)** the percentage of electroactive carbon in the HS fraction alog with the binding capacity of humic carbon for iron (BC_{HS} expressed in nmol-eqFe mgC^{-1}) at 20° 24.431'S, 166° 35.675'W at the TONGA station.

674 degradation of the biomass as previously demonstrated by Whitby et al. (2020a). High surface
675 eHS concentrations and their decrease with depth in the mesopelagic layer suggest that the
676 electroactivity of humic matter is a property affected by all the biogeochemical processes
677 governing the distribution of HS (e.g. surface production, bacterial degradation). The deep sea
678 concentrations of eHS were quite homogeneous (50 ± 12 µg-eqSRFA L^{-1}) indicating a partial
679 recalcitrance of the electroactivity to long term degradation. Conversion of eHS (in µg-
680 eqSRFA L^{-1}) into Fe-binding ligands of humic type (L_{FeHS}) can be estimated using the binding
681 capacity of the model humic-type ligand SRFA (1S101F) for dFe in seawater (14.6 ± 0.7
682 nmolFe $mgSRFA^{-1}$; Sukekava et al., 2018). A similar conversion is commonly used in the
683 recent literature (Dulaquais et al., 2018a, 2020; Laglera et al., 2019; Whitby et al., 2020a). At
684 this station we estimated L_{FeHS} values of between 0.3 and 2.4 nmol-eqFe L^{-1}. This interval fell
685 into the range of Fe-binding ligand (L_{Fe}) concentrations previously measured in the south

oligotrophic Pacific Ocean (0 – 4 nmol-eqFe L^{-1}; Buck et al., 2018; Cabanes et al., 2020). This result demonstrates that part of L_{Fe} were of humic nature.

In the oligotrophic Pacific Ocean, dFe is extremely depleted in surface waters (≤ 0.1 nM, Buck et al., 2018; Cabanes et al., 2020; Guieu et al., 2018). The implication of L_{FeHS} in the stabilization of surface dFe can be considered limited due to the possible occurrence of very strong iron binding ligands in this layer (e.g. siderophores, Boiteau et al., 2016). In contrast, in the deep ocean (> 1000 m) dFe exists at higher concentrations (> 0.4 nM). At these depths, intermediate iron chelators dominate (called L_2 in Buck et al., 2018) and humic-type ligands are thought to be a major component of this class of ligand (Bundy et al., 2015), therefore the role of humics in the stabilization of dFe is probably enhanced in the deep Pacific Ocean. To monitor the modifications of the binding properties of HS along with biogeochemical processes we determined the contribution of eHS to the HS fraction defined by SEC and estimated the binding capacity for Fe of humic DOC (BC_{HS}, Figure 6b). This calculation considers the carbon content of the SRFA standard used (52.44%) to normalize the concentrations expressed in µg eq-SRFA L^{-1} into µgC L^{-1} and assumes that all eHS elute in the HS fraction operationally defined by SEC (Riso et al., 2021). At this station the average contribution of eHS to the total HS carbon was ~ 9.1 ± 0.6 % (Figure 6b). This contribution varied along the water column with a maximum at 25 m (16.2%) and a minimum at 1089 m (4.1%). The non-constant contribution of eHS to HS DOC implies a non-conservativity of the binding properties of HS during their biogeochemical processing.

The BC_{HS} were systematically below those of the SRFA standard (BC_{SRFA} = 27.8 ± 1.3 nmol-eqFe mgC^{-1}) indicating a lower BC of marine humic carbon compared to the terrigenous humic matter. BC_{HS} in the shallowest sample (4.5 ± 0.1 nmol-eqFe mgC^{-1}) was significantly higher than in the deep sea (2.7 ± 0.5 nmol-eqFe mgC^{-1}; n = 6). A large part of HS in the upper 100 m depths was non-refractory (50%; Figure 3b), thereby we deduce that the binding capacity for dFe of non-refractory HS is higher than that of refractory HS. The decrease of the BC_{HS} from surface to 1089 m and the strong decrease of the contribution of eHS to humic DOC in the mesopelagic waters (Figure 6b) indicate an alteration of the Fe-binding properties during the microbial mineralization of HS DOC. Statistical analysis of the data did not reveal significant correlations between BC_{HS}, $\%C_{arom}$ nor the C:N elemental ratio of HS. This result suggests that Fe-binding moieties of marine HS are aliphatic and that the N-containing functional groups may not be involved in the formation of the Fe-humic complex in the marine environment. Based on these results, we suspect carboxylates to be the main chemical functional group involved in the Fe-binding properties of oceanic HS. Carboxylates are of

intermediate strength (Bundy et al., 2015) compared to N-containing (strong, Gledhill & Buck, 2012; Rue & Bruland, 1995) and aromatic/phenolic (weak, González et al., 2019) moieties for Fe complexation. The correlation between Fe-binding HS and CRAM in estuarine samples (Bundy et al., 2015) and the observations of humic type ligands falling into the intermediate class of Fe chelators (Buck et al., 2018; Bundy et al., 2015) both support this hypothesis. The decrease of BC_{HS} in the mesopelagic waters can be interpreted as a decrease of the abundance of carboxylates with HS during microbial transformation. This latter hypothesis is supported by the long-term experimental study (1 year) on the degradation of a large size spectra of DOM (108-7410 Da) by marine bacteria from Daoud & Trembley (2019). Their study showed a substantial decrease of carboxylate abundance in seawater DOM that suffered from microbial degradation compared to the control sample. There is currently no NMR data on oceanic HS samples to confirm this and the acquisition of such data along a full water column in the future would allow for the testing of this hypothesis.

Our results and interpretations of the complexation of dFe by humic matter contrast with terrestrial HS. For terrestrial HS, the binding capacity for dFe is thought to be linked to their aromaticity (Kikuchi et al., 2017) as it is observed in the two most used humic type standards SRFA ($\%C_{arom}$ = 24%; $BC_{SRFA\ 1S101F}$ = 14.6 nmolFe $mgSRFA^{-1}$; Sukekava et al., 2018) and SRHA ($\%C_{arom}$ = 37%; $BC_{SRHA\ 1S101H}$ = 31-32 nmolFe $mgSRHA^{-1}$; Abualhaija & van den Berg, 2014; Laglera & van den Berg, 2009). This difference further denotes the uniqueness of marine HS compared to terrestrial humic matter, as previously discussed by Malcolm (1990) in terms of chemical properties. We note that our results also contrast with Whitby et al. (2020b) where it was hypothesised that the Fe-binding capacities increased with depth due to higher HS aromaticity. In their study the higher Fe-binding capacities of HS in deep waters of the North Atlantic could be a result of a high fraction of terrestrial HS, in part derived from the subduction of humic-rich Arctic waters, which have been shown to have particularly high Fe-HS stability constants (Laglera et al., 2019). Lignin, an unambiguous molecular tracer for terrestrial DOC, is also higher in the Atlantic Ocean than in the Pacific Ocean (Hernes & Benner, 2002, 2006; Opsahl & Benner 1997). This suggests that the contribution of HS from terrestrial vs. marine sources could result in differences in Fe-complexing behaviour between oceanic regions.

4. Conclusions

This work presents the opportunity provided by multi-detection SEC to study the size-reactivity continuum and the chemical properties of oceanic DOC without any prior

extraction. This method has an excellent recovery of DOC and requires only a small sample volume (2.5 mL).

We used a combination of three semi-specific methods (SEC, fluorescence, CSV) to study DOM chemical modifications induced by biogeochemical processes along the water column of the oligotrophic Pacific Ocean. We identified N-contents of the BP and HS fractions as pools of bioavailable nitrogen. Our results also suggest the condensation, the decrease in N-content, the increase of quantum yield of fluorescence and a loss of complexing capacity for dFe of HS during microbial degradation of DOM. Marine HS seem to be produced in surface waters during biomass degradation. HS are initially non-refractory, nevertheless their ageing induces their transformation into refractory DOM. This process was identified to occur in two steps. First the microbial transformation in the mesopelagic waters increases their aromaticity and their fluorescence, secondly, long term (> centuries) processing alters their aromatic content making marine HS more aliphatic. All these changes in the chemical properties could alter and gradually degrade the newly produced labile DOM into RDOM trapped in the deep ocean. This work provides insights to reconcile the quantitative (loss of matter) and qualitative (increase of fluorescence) views in humic oceanic biogeochemistry.

Results of this work and the conclusions drawn are consistent with studies that used molecular approaches to characterize fate of DOM in field samples (Osterholz et al., 2021) and in bacterial incubation experiments (Lian et al., 2021; Zheng et al., 2019). A larger scale study and the use of a molecular approach to each DOM fraction isolated in this work would confirm the main hypotheses.

Acknowledgments

We would like to thank Vincent Taillandier for providing CTD data for the TONGA GPpr14 cruise. CTD data from the TONGA expedition are available at http://www.obs-vlfr.fr/proof/php/TONGA/tonga.php. We acknowledge the dedicated sea-going staff of the Ocean Data Facility of S.I.O for generating high quality and calibrated CTD data during the US-GP15 expedition. CTD data from the US-GP15 cruise are available at https://cchdo.ucsd.edu/cruise/33RR20180918. CTD data from the CLIVAR-P16 expedition are available at https://www.bco-dmo.org/dataset/778403. We warmly thank captains and crew of R/V *L'Atalante* and *Roger Revelle*, as well as chief scientists Karen Casciotti, Greg Cutter & Phoebe Lam of the US-GP15 expedition, Cécile Guieu & Sophie Bonnet of the TONGA expedition, and the scientific crews of both expeditions for their work at sea and sample collection. We especially thank Matthieu Bressac, Veronica Arnone and David González-Santana for sampling during the TONGA cruise. We are grateful to Karen Casciotti

for her valuable assistance to get GEOTRACES samples. We warmly thank Pascal Annabelle Baya for subsampling of GEOTRACES samples. We also thank the PACEM platform for the Mediterranean Institute of Oceanography. We thank Millie Goddard-Dwyer for assistance in editing and reviewing. This work is part of the BioDOMPO project (PI. Gabriel Dulaquais), funded by the French National program LEFE (*Les enveloppes Fluides et l'Environnement*) Cyber of the CNRS and ISblue (www.isblue.fr). This work is part of the TONGA project (ANR-18-CE1-0016, CNRS, IRD, Ifremer). The PhD grant of Pierre Fourrier was funded by ISblue and région Bretagne. This work was conducted in the framework of the GEOTRACES program.

References

Abualhaija, M. M., & van den Berg, C. M. (2014). Chemical speciation of iron in seawater using catalytic cathodic stripping voltammetry with ligand competition against salicylaldoxime. *Marine Chemistry*, *164*, 60-74. https://doi.org/10.1016/j.marchem.2014.06.005.

Aiken, G. R., Brown, P. A., Noyes, T. I., & Pinckney, D. J. (1989). Molecular size and weight of fulvic and humic acids from the Suwannee River. *Humic substances in the Suwannee River, Georgia: Interactions, properties, and proposed structures*, 87-557.

Aminot, A., & Kérouel, R. (2004). Dissolved organic carbon, nitrogen and phosphorus in the NE Atlantic and the NW Mediterranean with particular reference to non-refractory fractions and degradation. *Deep Sea Research Part I: Oceanographic Research Papers*, *51*(12), 1975-1999. https://doi.org/10.1016/j.dsr.2004.07.016

Amon, R. M., & Benner, R. (1994). Rapid cycling of high-molecular-weight dissolved organic matter in the ocean. *Nature*, *369*(6481), 549-552. https://doi.org/10.1038/369549a0

Amon, R. M., & Benner, R. (1996). Bacterial utilization of different size classes of dissolved organic matter. *Limnology and Oceanography*, *41*(1), 41-51. https://doi.org/10.4319/lo.1996.41.1.0041

Amy, G., & Her, N. (2004). Size exclusion chromatography (SEC) with multiple detectors: a powerful tool in treatment process selection and performance monitoring. *Water science and technology: Water supply*, *4*(4), 19-24. https://doi.org/10.2166/ws.2004.0056

Arrieta, J. M., Mayol, E., Hansman, R. L., Herndl, G. J., Dittmar, T., & Duarte, C. M. (2015). Dilution limits dissolved organic carbon utilization in the deep ocean. *Science*, *348*(6232), 331-333. https://doi.org/10.1126/science.1258955

Ateia, M., Ran, J., Fujii, M., & Yoshimura, C. (2017). The relationship between molecular composition and fluorescence properties of humic substances. *International Journal of Environmental Science and Technology*, *14*(4), 867-880. https://doi.org/10.1007/s13762-016-1214-x

Baghoth, S. A., Maeng, S. K., Rodriguez, S. S., Ronteltap, M., Sharma, S., Kennedy, M., & Amy, G. L. (2008). An urban water cycle perspective of natural organic matter (NOM): NOM in drinking water, wastewater effluent, storm water, and seawater. Water Science and Technology: Water Supply, 8(6), 701-707. https://doi.org/10.2166/ws.2008.146

Becker, S.& Swift, J. 2020. CTD data from Cruise 33RR20180918, exchange version. Accessed from CCHDO https://cchdo.ucsd.edu/cruise/33RR20180918. Access date 2021-01-05.

Benner, R. (2003). Molecular indicators of the bioavailability of dissolved organic matter. In *Aquatic ecosystems* (pp. 121-137). Academic Press. https://doi.org/10.1016/B978-012256371-3/50006-8

Benner, R., & Amon, R. M. (2015). The size-reactivity continuum of major bioelements in the ocean. Annual review of marine science, 7, 185-205. https://doi.org/10.1146/annurev-marine-010213-135126

Bercovici, S. K., & Hansell, D. A. (2016). Dissolved organic carbon in the deep Southern Ocean: Local versus distant controls. *Global Biogeochemical Cycles*, *30*(2), 350-360. https://doi.org/10.1002/2015GB005252

Birdwell, J. E., & Engel, A. S. (2010). Characterization of dissolved organic matter in cave and spring waters using UV–Vis absorbance and fluorescence spectroscopy. *Organic Geochemistry*, *41*(3), 270-280. https://doi.org/10.1016/j.orggeochem.2009.11.002

Boiteau, R. M., Mende, D. R., Hawco, N. J., McIlvin, M. R., Fitzsimmons, J. N., Saito, M. A., ... & Repeta, D. J. (2016). Siderophore-based microbial adaptations to iron scarcity across the eastern Pacific Ocean. *Proceedings of the National Academy of Sciences*, *113*(50), 14237-14242. https://doi.org/10.1073/pnas.1608594113

Buck, K. N., Sedwick, P. N., Sohst, B., & Carlson, C. A. (2018). Organic complexation of iron in the eastern tropical South Pacific: results from US GEOTRACES Eastern Pacific Zonal Transect (GEOTRACES cruise GP16). *Marine Chemistry*, *201*, 229-241. https://doi.org/10.1016/j.marchem.2017.11.007

Bundy, R. M., Abdulla, H. A., Hatcher, P. G., Biller, D. V., Buck, K. N., & Barbeau, K. A. (2015). Iron-binding ligands and humic substances in the San Francisco Bay estuary and estuarine-influenced shelf regions of coastal California. *Marine Chemistry*, *173*, 183-194. https://doi.org/10.1016/j.marchem.2014.11.005

Burdige, D. J., Kline, S. W., & Chen, W. (2004). Fluorescent dissolved organic matter in marine sediment pore waters. Marine Chemistry, 89(1-4), 289-311. https://doi.org/10.1016/j.marchem.2004.02.015

Cabanes, D. J., Norman, L., Bowie, A. R., Strmečki, S., & Hassler, C. S. (2020). Electrochemical evaluation of iron-binding ligands along the Australian GEOTRACES southwestern Pacific section (GP13). *Marine Chemistry*, *219*, 103736. https://doi.org/10.1016/j.marchem.2019.103736

Chen, M., & Hur, J. (2015). Pre-treatments, characteristics, and biogeochemical dynamics of dissolved organic matter in sediments: A review. *water research*, *79*, 10-25. https://doi.org/10.1016/j.watres.2015.04.018

Chen, W. B., Smith, D. S., & Guéguen, C. (2013). Influence of water chemistry and dissolved organic matter (DOM) molecular size on copper and mercury binding determined by multiresponse fluorescence quenching. *Chemosphere*, *92*(4), 351-359. https://doi.org/10.1016/j.chemosphere.2012.12.075

Chen, M., Nam, S. I., Kim, J. H., Kwon, Y. J., Hong, S., Jung, J., ... & Hur, J. (2017). High abundance of protein-like fluorescence in the Amerasian Basin of Arctic Ocean: Potential implication of a fall phytoplankton bloom. *Science of the Total Environment*, *599*, 355-363. https://doi.org/10.1016/j.scitotenv.2017.04.233

Coble, P. G. (1996). Characterization of marine and terrestrial DOM in seawater using excitation-emission matrix spectroscopy. Marine chemistry, 51(4), 325-346. https://doi.org/10.1016/0304-4203(95)00062-3

Coble, P. G. (2007). Marine optical biogeochemistry: the chemistry of ocean color. *Chemical reviews*, *107*(2), 402-418. https://doi.org/10.1021/cr050350+

Coppola, A. I., & Druffel, E. R. (2016). Cycling of black carbon in the ocean. *Geophysical Research Letters*, *43*(9), 4477-4482. https://doi.org/10.1002/2016GL068574

Corin, N., Backlund, P., & Kulovaara, M. (1996). Degradation products formed during UV-irradiation of humic waters. *Chemosphere*, *33*(2), 245-255. https://doi.org/10.1016/0045-6535(96)00167-1

Cornelissen, E. R., Moreau, N., Siegers, W. G., Abrahamse, A. J., Rietveld, L. C., Grefte, A., ... & Wessels, L. P. (2008). Selection of anionic exchange resins for removal of natural organic matter (NOM) fractions. *Water research*, *42*(1-2), 413-423. https://doi.org/10.1016/j.watres.2007.07.033

Cutter, G. A., Scientists, C. C., Casciotti, K. L., & Lam, P. J. (2018). US GEOTRACES Pacific Meridional Transect–GP15 Cruise Report.

Daoud, A. B. A., & Tremblay, L. (2019). HPLC-SEC-FTIR characterization of the dissolved organic matter produced by the microbial carbon pump. *Marine Chemistry*, *215*, 103668. https://doi.org/10.1016/j.marchem.2019.103668

Del Vecchio, R., & Blough, N. V. (2002). Photobleaching of chromophoric dissolved organic matter in natural waters: kinetics and modeling. *Marine Chemistry*, *78*(4), 231-253. https://doi.org/10.1016/S0304-4203(02)00036-1

Dhakal, N., Salinas-Rodriguez, S. G., Ouda, A., Schippers, J. C., & Kennedy, M. D. (2018). Fouling of ultrafiltration membranes by organic matter generated by marine algal species. *Journal of Membrane Science*, *555*, 418-428. https://doi.org/10.1016/j.memsci.2018.03.057

Dittmar, T. (2008). The molecular level determination of black carbon in marine dissolved organic matter. *Organic Geochemistry*, *39*(4), 396-407. https://doi.org/10.1016/j.orggeochem.2008.01.015

Dittmar, T., & Kattner, G. (2003). The biogeochemistry of the river and shelf ecosystem of the Arctic Ocean: a review. *Marine chemistry*, *83*(3-4), 103-120. https://doi.org/10.1016/S0304-4203(03)00105-1

Dittmar, T., & Koch, B. P. (2006). Thermogenic organic matter dissolved in the abyssal ocean. *Marine Chemistry*, *102*(3-4), 208-217. https://doi.org/10.1016/j.marchem.2006.04.003

Dittmar, T., & Paeng, J. (2009). A heat-induced molecular signature in marine dissolved organic matter. *Nature Geoscience*, *2*(3), 175-179. https://doi.org/10.1038/ngeo440

Druffel, E. R., Williams, P. M., Bauer, J. E., & Ertel, J. R. (1992). Cycling of dissolved and particulate organic matter in the open ocean. *Journal of Geophysical Research: Oceans*, *97*(C10), 15639-15659. https://doi.org/10.1029/92JC01511

Dulaquais, G., Breitenstein, J., Waeles, M., Marsac, R., & Riso, R. (2018b). Measuring dissolved organic matter in estuarine and marine waters: size-exclusion chromatography with various detection methods. *Environmental Chemistry*, *15*(7), 436-449. https://doi.org/10.1071/EN18108

Dulaquais, G., Waeles, M., Breitenstein, J., Knoery, J., & Riso, R. (2020). Links between size fractionation, chemical speciation of dissolved copper and chemical speciation of dissolved organic matter in the Loire estuary. *Environmental Chemistry*, *17*(5), 385-399. https://doi.org/10.1071/EN19137

Dulaquais, G., Waeles, M., Gerringa, L. J., Middag, R., Rijkenberg, M. J., & Riso, R. (2018a). The biogeochemistry of electroactive humic substances and its connection to iron chemistry in the North East Atlantic and the Western Mediterranean Sea. *Journal of Geophysical Research: Oceans*, *123*(8), 5481-5499. https://doi.org/10.1029/2018JC014211

Ertel, J. R., Hedges, J. I., & Perdue, E. M. (1984). Lignin signature of aquatic humic substances. *Science*, *223*(4635), 485-487. https://doi.org/10.1126/science.223.4635.485

Esteves, V. I., Otero, M., & Duarte, A. C. (2009). Comparative characterization of humic substances from the open ocean, estuarine water and fresh water. Organic Geochemistry, 40(9), 942-950. https://doi.org/10.1016/j.orggeochem.2009.06.006

Fellman, J. B., Hood, E., & Spencer, R. G. (2010). Fluorescence spectroscopy opens new windows into dissolved organic matter dynamics in freshwater ecosystems: A review. *Limnology and oceanography*, *55*(6), 2452-2462. https://doi.org/10.4319/lo.2010.55.6.2452

Fichot, C. G., & Benner, R. (2011). A novel method to estimate DOC concentrations from CDOM absorption coefficients in coastal waters. *Geophysical research letters*, *38*(3). https://doi.org/10.1029/2010GL046152

Fumenia, A., Moutin, T., Bonnet, S., Benavides, M., Petrenko, A., Helias Nunige, S., & Maes, C. (2018). Excess nitrogen as a marker of intense dinitrogen fixation in the Western Tropical South Pacific Ocean: impact on the thermocline waters of the South Pacific. *Biogeosciences Discussions*, 1-33. https://doi.org/10.5194/bg-2017-557

Gaid, K. (2011). A Large Review of Pretreatment. *Expanding issues in desalination*. https://doi.org/10.5772/19680

Gao, Z., & Guéguen, C. (2018). Distribution of thiol, humic substances and colored dissolved organic matter during the 2015 Canadian Arctic GEOTRACES cruises. Marine Chemistry, 203, 1-9. https://doi.org/10.1016/j.marchem.2018.04.001

Gledhill, M., & Buck, K. N. (2012). The organic complexation of iron in the marine environment: a review. *Frontiers in microbiology*, *3*, 69. https://doi.org/10.3389/fmicb.2012.00069

González, A. G., Cadena-Aizaga, M. I., Sarthou, G., González-Dávila, M., & Santana-Casiano, J. M. (2019). Iron complexation by phenolic ligands in seawater. *Chemical geology*, *511*, 380-388. https://doi.org/10.1016/j.chemgeo.2018.10.017

Green, N. W., Perdue, E. M., Aiken, G. R., Butler, K. D., Chen, H., Dittmar, T., ... & Stubbins, A. (2014). An intercomparison of three methods for the large-scale isolation of oceanic dissolved organic matter. Marine Chemistry, 161, 14-19. https://doi.org/10.1016/j.marchem.2014.01.012

Gu, B., Schmitt, J., Chen, Z., Liang, L., & McCarthy, J. F. (1995). Adsorption and desorption of different organic matter fractions on iron oxide. *Geochimica et cosmochimica acta*, *59*(2), 219-229. https://doi.org/10.1016/0016-7037(94)00282-Q

Guieu, C., Bonnet, S. (2019). TONGA Cruise Report. https://doi.org/10.17600/18000884

Guieu, C., Bonnet, S., Petrenko, A., Menkes, C., Chavagnac, V., Desboeufs, K., ... & Moutin, T. (2018). Iron from a submarine source impacts the productive layer of the Western Tropical South Pacific (WTSP). *Scientific reports*, *8*(1), 1-9. https://doi.org/10.1073/pnas.1619514114

Hach, P. F., Marchant, H. K., Krupke, A., Riedel, T., Meier, D. V., Lavik, G., ... & Kuypers, M. M. (2020). Rapid microbial diversification of dissolved organic matter in oceanic surface waters leads to carbon sequestration. *Scientific reports*, *10*(1), 1-10. https://doi.org/10.1038/s41598-020-69930-y

Hansell, D. A., Carlson, C. A., Repeta, D. J., & Schlitzer, R. (2009). Dissolved organic matter in the ocean: A controversy stimulates new insights. *Oceanography*, *22*(4), 202-211. https://doi.org/10.5670/oceanog.2009.109

Hartin, C. A., Fine, R. A., Sloyan, B. M., Talley, L. D., Chereskin, T. K., & Happell, J. (2011). Formation rates of Subantarctic mode water and Antarctic intermediate water within the South Pacific. *Deep Sea Research Part I: Oceanographic Research Papers*, *58*(5), 524-534. https://doi.org/10.1016/j.dsr.2011.02.010

Harvey, G. R., Boran, D. A., Chesal, L. A., & Tokar, J. M. (1983). The structure of marine fulvic and humic acids. *Marine Chemistry*, *12*(2-3), 119-132. https://doi.org/10.1016/0304-4203(83)90075-0

Hawco, N. J., Lam, P. J., Lee, J. M., Ohnemus, D. C., Noble, A. E., Wyatt, N. J., ... & Saito, M. A. (2018). Cobalt scavenging in the mesopelagic ocean and its influence on global mass balance: Synthesizing water column and sedimentary fluxes. *Marine Chemistry*, *201*, 151-166. https://doi.org/10.1016/j.marchem.2017.09.001

Hedges, J. I., Hatcher, P. G., Ertel, J. R., & Meyers-Schulte, K. J. (1992). A comparison of dissolved humic substances from seawater with Amazon River counterparts by 13C-NMR spectrometry. *Geochimica et Cosmochimica Acta*, *56*(4), 1753-1757. https://doi.org/10.1016/0016-7037(92)90241-A

Helms, J. R., Mao, J., Stubbins, A., Schmidt-Rohr, K., Spencer, R. G., Hernes, P. J., & Mopper, K. (2014). Loss of optical and molecular indicators of terrigenous dissolved organic matter during long-term photobleaching. *Aquatic sciences*, *76*(3), 353-373. https://doi.org/10.1007/s00027-014-0340-0

Helms, J. R., Stubbins, A., Perdue, E. M., Green, N. W., Chen, H., & Mopper, K. (2013). Photochemical bleaching of oceanic dissolved organic matter and its effect on absorption spectral slope and fluorescence. *Marine Chemistry*, *155*, 81-91. https://doi.org/10.1016/j.marchem.2013.05.015

Hernes, P. J., & Benner, R. (2002). Transport and diagenesis of dissolved and particulate terrigenous organic matter in the North Pacific Ocean. *Deep Sea Research Part I: Oceanographic Research Papers*, *49*(12), 2119-2132. https://doi.org/10.1016/S0967-0637(02)00128-0

Hernes, P. J., & Benner, R. (2006). Terrigenous organic matter sources and reactivity in the North Atlantic Ocean and a comparison to the Arctic and Pacific oceans. *Marine Chemistry*, *100*(1-2), 66-79. https://doi.org/10.1016/j.marchem.2005.11.003

Hertkorn, N., Benner, R., Frommberger, M., Schmitt-Kopplin, P., Witt, M., Kaiser, K., ... & Hedges, J. I. (2006). Characterization of a major refractory component of marine dissolved organic matter. *Geochimica et Cosmochimica Acta*, *70*(12), 2990-3010. https://doi.org/10.1016/j.gca.2006.03.021

Hertkorn, N., Harir, M., Koch, B., Michalke, B., & Schmitt-Kopplin, P. (2013). High-field NMR spectroscopy and FTICR mass spectrometry: powerful discovery tools for the molecular level characterization of marine dissolved organic matter. *Biogeosciences*, *10*, 1583-1624. https://doi.org/10.5194/bg-10-1583-2013

Hessen, D., & Tranvik, L. J. (Eds.). (2013). *Aquatic humic substances: ecology and biogeochemistry* (Vol. 133). Springer Science & Business Media. https://doi.org/10.1007/978-3-662-03736-2

Hoge, F. E., Vodacek, A., & Blough, N. V. (1993). Inherent optical properties of the ocean: retrieval of the absorption coefficient of chromophoric dissolved organic matter from fluorescence measurements. *Limnology and Oceanography*, *38*(7), 1394-1402. https://doi.org/10.4319/lo.1993.38.7.1394

Huber, S. A., Balz, A., Abert, M., & Pronk, W. (2011). Characterisation of aquatic humic and non-humic matter with size-exclusion chromatography–organic carbon detection–organic nitrogen detection (LC-OCD-OND). *Water research*, *45*(2), 879-885. https://doi.org/10.1016/j.watres.2010.09.023

Huber, S. A., & Frimmel, F. H. (1994). Direct gel chromatographic characterization and quantification of marine dissolved organic carbon using high-sensitivity DOC detection. *Environmental science & technology*, *28*(6), 1194-1197. https://doi.org/10.1021/es00055a035

Hudson, N., Baker, A., & Reynolds, D. (2007). Fluorescence analysis of dissolved organic matter in natural, waste and polluted waters—a review. *River research and applications*, *23*(6), 631-649. https://doi.org/10.1002/rra.1005

Huguet, A., Vacher, L., Relexans, S., Saubusse, S., Froidefond, J. M., & Parlanti, E. (2009). Properties of fluorescent dissolved organic matter in the Gironde Estuary. Organic Geochemistry, 40(6), 706-719. https://doi.org/10.1016/j.orggeochem.2009.03.002

Jiao, N., Herndl, G. J., Hansell, D. A., Benner, R., Kattner, G., Wilhelm, S. W., ... & Azam, F. (2010). Microbial production of recalcitrant dissolved organic matter: long-term carbon storage in the global ocean. *Nature Reviews Microbiology*, *8*(8), 593-599. https://doi.org/10.1038/nrmicro2386

Kalbitz, K., Schwesig, D., Schmerwitz, J., Kaiser, K., Haumaier, L., Glaser, B., ... & Leinweber, P. (2003). Changes in properties of soil-derived dissolved organic matter induced by biodegradation. *Soil Biology and Biochemistry*, *35*(8), 1129-1142. https://doi.org/10.1016/S0038-0717(03)00165-2

Kähler, P., & Koeve, W. (2001). Marine dissolved organic matter: can its C: N ratio explain carbon overconsumption?. *Deep Sea Research Part I: Oceanographic Research Papers*, *48*(1), 49-62. https://doi.org/10.1016/S0967-0637(00)00034-0

Kieber, R. J., Hydro, L. H., & Seaton, P. J. (1997). Photooxidation of triglycerides and fatty acids in seawater: Implication toward the formation of marine humic substances. *Limnology and Oceanography*, *42*(6), 1454-1462. https://doi.org/10.4319/lo.1997.42.6.1454

Kikuchi, T., Fujii, M., Terao, K., Jiwei, R., Lee, Y. P., & Yoshimura, C. (2017). Correlations between aromaticity of dissolved organic matter and trace metal concentrations in natural and effluent waters: A case study in the Sagami River Basin, Japan. *Science of the Total Environment*, *576*, 36-45. https://doi.org/10.1016/j.scitotenv.2016.10.068

Kinsey, J. D., Corradino, G., Ziervogel, K., Schnetzer, A., & Osburn, C. L. (2018). Formation of chromophoric dissolved organic matter by bacterial degradation of phytoplankton-derived aggregates. *Frontiers in Marine Science*, *4*, 430. https://doi.org/10.3389/fmars.2017.00430

Koshlyakov, M. N., & Tarakanov, R. Y. (1999). Water masses of the Pacific Antarctic. Oceanology, 39(1), 1-11. https://doi.org/10.1029/2007JC004549

Kowalenko, C. G., & McKercher, R. B. (1971). Phospholipid components extracted from Saskatchewan soils. *Canadian Journal of Soil Science*, *51*(1), 19-22. https://doi.org/10.4141/cjss71-003

Kujawinski, E. B. (2011). The impact of microbial metabolism on marine dissolved organic matter. *Annual review of marine science*, *3*, 567-599. https://doi.org/10.1146/annurev-marine-120308-081003

Kujawinski, E. B., Longnecker, K., Blough, N. V., Del Vecchio, R., Finlay, L., Kitner, J. B., & Giovannoni, S. J. (2009). Identification of possible source markers in marine dissolved organic matter using ultrahigh resolution mass spectrometry. *Geochimica et Cosmochimica Acta*, *73*(15), 4384-4399. https://doi.org/10.1016/j.gca.2009.04.033

Laglera, L. M., Battaglia, G., & van den Berg, C. M. (2007). Determination of humic substances in natural waters by cathodic stripping voltammetry of their complexes with iron. *Analytica chimica acta*, *599*(1), 58-66. https://doi.org/10.1016/j.aca.2007.07.059

Laglera, L. M., Sukekava, C., Slagter, H. A., Downes, J., Aparicio-Gonzalez, A., & Gerringa, L. J. (2019). First quantification of the controlling role of humic substances in the transport of iron across the surface of the Arctic Ocean. *Environmental science & technology*, *53*(22), 13136-13145. https://doi.org/10.1021/acs.est.9b04240

Laglera, L. M., & van den Berg, C. M. (2009). Evidence for geochemical control of iron by humic substances in seawater. *Limnology and Oceanography*, *54*(2), 610-619. https://doi.org/10.4319/lo.2009.54.2.0610

Lahajnar, N., Rixen, T., Gaye-Haake, B., Schäfer, P., & Ittekkot, V. (2005). Dissolved organic carbon (DOC) fluxes of deep-sea sediments from the Arabian Sea and NE Atlantic. *Deep Sea Research Part II: Topical Studies in Oceanography*, *52*(14-15), 1947-1964. https://doi.org/10.1016/j.dsr2.2005.05.006

Lara, R. J., Hubberten, U., & Kattner, G. (1993). Contribution of humic substances to the dissolved nitrogen pool in the Greenland Sea. *Marine chemistry*, *41*(4), 327-336. https://doi.org/10.1016/0304-4203(93)90264-O

Lehmann, J., & Kleber, M. (2015). The contentious nature of soil organic matter. *Nature*, *528*(7580), 60-68. https://doi.org/10.1038/nature16069

Letscher, R. T., & Moore, J. K. (2015). Preferential remineralization of dissolved organic phosphorus and non-Redfield DOM dynamics in the global ocean: Impacts on marine productivity, nitrogen fixation, and carbon export. *Global Biogeochemical Cycles*, *29*(3), 325-340. https://doi.org/10.1002/2014GB004904

Lian, J., Zheng, X., Zhuo, X., Chen, Y. L., He, C., Zheng, Q., ... & Cai, R. (2021). Microbial transformation of distinct exogenous substrates into analogous composition of recalcitrant dissolved organic matter. *Environmental Microbiology*, *23*(5), 2389-2403. https://doi.org/10.1111/1462-2920.15426

Mackenzie, F. T. (1981). Global carbon cycle: Some minor sinks for CO_2, in Flux of Organic Carbon by Rivers to the Oceans, edited by G. E. Likens, F. T. MacKenzie, J. E. Richey, J. R. Sedell, and K. K. Turekian, pp. 360-384, U.S. Department of Energy, Washington, D.C.

Maillard, L. C. (1912). Condensation des acides aminés sur les sucres; formation de melanoïdines par voie méthodique. *CR Acad Sci Paris*, *154*, 66-8.

Malcolm, R. L. (1990). The uniqueness of humic substances in each of soil, stream and marine environments. *Analytica Chimica Acta*, *232*, 19-30. https://doi.org/10.1016/S0003-2670(00)81222-2

Marques, J. S., Dittmar, T., Niggemann, J., Almeida, M. G., Gomez-Saez, G. V., & Rezende, C. E. (2017). Dissolved black carbon in the headwaters-to-ocean continuum of Paraiba Do Sul River, Brazil. *Frontiers in Earth Science*, *5*, 11. https://doi.org/10.3389/feart.2017.00011

McCartney, M. S. (1979). Subantarctic mode water. *Woods Hole Oceanographic Institution Contribution*, *3773*, 103-119.

McKnight, D. M., Boyer, E. W., Westerhoff, P. K., Doran, P. T., Kulbe, T., & Andersen, D. T. (2001). Spectrofluorometric characterization of dissolved organic matter for indication of precursor organic material and aromaticity. Limnology and Oceanography, 46(1), 38-48. https://doi.org/10.4319/lo.2001.46.1.0038

Medeiros, P. M., Seidel, M., Powers, L. C., Dittmar, T., Hansell, D. A., & Miller, W. L. (2015). Dissolved organic matter composition and photochemical transformations in the northern North Pacific Ocean. *Geophysical Research Letters*, *42*(3), 863-870. https://doi.org/10.1002/2014GL062663

Menzel, D. W., & Vaccaro, R. F. (1964). The measurement of dissolved organic and particulate carbon in seawater 1. *Limnology and Oceanography*, *9*(1), 138-142. https://doi.org/10.4319/lo.1964.9.1.0138

Miranda, M. L., Mustaffa, N. I. H., Robinson, T. B., Stolle, C., Ribas-Ribas, M., Wurl, O., ... & Blomquist, B. (2018). Influence of solar radiation on biogeochemical parameters and fluorescent dissolved organic matter (FDOM) in the sea surface microlayer of the southern coastal North Sea. *Elementa: Science of the Anthropocene*, *6*. https://doi.org/10.1525/elementa.278

Miranda, M. L., Osterholz, H., Giebel, H. A., Bruhnke, P., Dittmar, T., & Zielinski, O. (2020). Impact of UV radiation on DOM transformation on molecular level using FT-ICR-MS and PARAFAC. *Spectrochimica Acta Part A: Molecular and Biomolecular Spectroscopy*, *230*, 118027. https://doi.org/10.1016/j.saa.2020.118027

Mopper, K., Stubbins, A., Ritchie, J. D., Bialk, H. M., & Hatcher, P. G. (2007). Advanced instrumental approaches for characterization of marine dissolved organic matter: extraction techniques, mass spectrometry, and nuclear magnetic resonance spectroscopy. *Chemical Reviews*, *107*(2), 419-442. https://doi.org/10.1021/cr050359b

Nakane, M., Ajioka, T., & Yamashita, Y. (2017). Distribution and sources of dissolved black carbon in surface waters of the Chukchi Sea, Bering Sea, and the North Pacific Ocean. *Frontiers in earth science*, *5*, 34. https://doi.org/10.3389/feart.2017.00034

Ogawa, H., & Tanoue, E. (2003). Dissolved organic matter in oceanic waters. *Journal of Oceanography*, *59*(2), 129-147. https://doi.org/10.1023/A:1025528919771

Ohno, T., Chorover, J., Omoike, A., & Hunt, J. (2007). Molecular weight and humification index as predictors of adsorption for plant-and manure-derived dissolved organic matter to goethite. European Journal of Soil Science, 58(1), 125-132. https://doi.org/10.1111/j.1365-2389.2006.00817.x

Opsahl, S., & Benner, R. (1997). Distribution and cycling of terrigenous dissolved organic matter in the ocean. *Nature*, *386*(6624), 480-482. https://doi.org/10.1038/386480a0

Osburn, C. L., Boyd, T. J., Montgomery, M. T., Bianchi, T. S., Coffin, R. B., & Paerl, H. W. (2016). Optical proxies for terrestrial dissolved organic matter in estuaries and coastal waters. *Frontiers in Marine Science*, *2*, 127. https://doi.org/10.3389/fmars.2015.00127

Osburn, C. L., Kinsey, J. D., Bianchi, T. S., & Shields, M. R. (2019). Formation of planktonic chromophoric dissolved organic matter in the ocean. *Marine Chemistry*, *209*, 1-13. https://doi.org/10.1016/j.marchem.2018.11.010

Osterholz, H., Kilgour, D. P., Storey, D. S., Lavik, G., Ferdelman, T. G., Niggemann, J., & Dittmar, T. (2021). Accumulation of DOC in the South Pacific Subtropical Gyre from a molecular perspective. *Marine Chemistry*, *231*, 103955. https://doi.org/10.1016/j.marchem.2021.103955

Para, J., Coble, P. G., Charrière, B., Tedetti, M., Fontana, C., & Sempere, R. (2010). Fluorescence and absorption properties of chromophoric dissolved organic matter (CDOM) in coastal surface waters of the

northwestern Mediterranean Sea, influence of the Rhône River. *Biogeosciences*, *7*(12), 4083-4103. https://doi.org/10.5194/bg-7-4083-2010

Paerl, R. W., Claudio, I. M., Shields, M. R., Bianchi, T. S., & Osburn, C. L. (2020). Dityrosine formation via reactive oxygen consumption yields increasingly recalcitrant humic-like fluorescent organic matter in the ocean. *Limnology and Oceanography Letters*, *5*(5), 337-345. https://doi.org/10.1002/lol2.10154

Parlanti, E., Wörz, K., Geoffroy, L., & Lamotte, M. (2000). Dissolved organic matter fluorescence spectroscopy as a tool to estimate biological activity in a coastal zone submitted to anthropogenic inputs. Organic geochemistry, 31(12), 1765-1781. https://doi.org/10.1016/S0146-6380(00)00124-8

Peters, B. D., Jenkins, W. J., Swift, J. H., German, C. R., Moffett, J. W., Cutter, G. A., ... & Casciotti, K. L. (2018). Water mass analysis of the 2013 US GEOTRACES eastern Pacific zonal transect (GP16). *Marine Chemistry*, *201*, 6-19. https://doi.org/10.1016/j.marchem.2017.09.007

Polimene, L., Rivkin, R. B., Luo, Y. W., Kwon, E. Y., Gehlen, M., Pena, M. A., ... & Jiao, N. (2018). Modelling marine DOC degradation time scales. *National Science Review*, *5*(4), 468-474. https://doi.org/10.1093/nsr/nwy066

Poulin, B. A., Ryan, J. N., & Aiken, G. R. (2014). Effects of iron on optical properties of dissolved organic matter. Environmental Science &Technology,48(17), 10,098–10,106. https://doi.org/10.1021/es502670r

Powell, R. T., & Donat, J. R. (2001). Organic complexation and speciation of iron in the South and Equatorial Atlantic. *Deep Sea Research Part II: Topical Studies in Oceanography*, *48*(13), 2877-2893. https://doi.org/10.1016/S0967-0645(01)00022-4

Repeta, D. J., Quan, T. M., Aluwihare, L. I., & Accardi, A. (2002). Chemical characterization of high molecular weight dissolved organic matter in fresh and marine waters. *Geochimica et Cosmochimica Acta*, *66*(6), 955-962. https://doi.org/10.1016/S0016-7037(01)00830-4

Riso, R., Mastin, M., Aschehoug, A., Davy, R., Devesa, J., Laës-Huon, A, Waeles, M. & Dulaquais, G. (2021). Distribution, speciation and composition of humic substances in a macro-tidal temperate estuary. *Estuarine, Coastal and Shelf Science*, 107360. https://doi.org/10.1016/j.ecss.2021.107360

Rue, E. L., & Bruland, K. W. (1995). Complexation of iron (III) by natural organic ligands in the Central North Pacific as determined by a new competitive ligand equilibration/adsorptive cathodic stripping voltammetric method. *Marine chemistry*, *50*(1-4), 117-138. https://doi.org/10.1016/0304-4203(95)00031-L

Rue, E. L., & Bruland, K. W. (1997). The role of organic complexation on ambient iron chemistry in the equatorial Pacific Ocean and the response of a mesoscale iron addition experiment. *Limnology and oceanography*, *42*(5), 901-910. https://doi.org/10.4319/lo.1997.42.5.0901

Segnini, A., Posadas, A., Quiroz, R., Milori, D. M. B. P., Saab, S. C., Neto, L. M., & Vaz, C. M. P. (2010). Spectroscopic assessment of soil organic matter in wetlands from the high Andes. *Soil Science Society of America Journal*, *74*(6), 2246-2253. https://doi.org/10.2136/sssaj2009.0445

Shen, Y., & Benner, R. (2018). Mixing it up in the ocean carbon cycle and the removal of refractory dissolved organic carbon. *Scientific reports*, *8*(1), 1-9. https://doi.org/10.1038/s41598-018-20857-5

Shen, Y., & Benner, R. (2020). Molecular properties are a primary control on the microbial utilization of dissolved organic matter in the ocean. *Limnology and Oceanography*, *65*(5), 1061-1071. https://doi.org/10.1002/lno.11369

Silva, N., Rojas, N., & Fedele, A. (2009). Water masses in the Humboldt Current System: Properties, distribution, and the nitrate deficit as a chemical water mass tracer for Equatorial Subsurface Water off Chile. *Deep Sea Research Part II: Topical Studies in Oceanography*, *56*(16), 1004-1020. https://doi.org/10.1016/j.dsr2.2008.12.013

Slagter, H. A., Laglera, L. M., Sukekava, C., & Gerringa, L. J. (2019). Fe-binding organic ligands in the humic-rich TransPolar Drift in the surface Arctic Ocean using multiple voltammetric methods. Journal of Geophysical Research: Oceans, 124(3), 1491-1508. https://doi.org/10.1029/2018JC014576

Sohrin, R., & Sempéré, R. (2005). Seasonal variation in total organic carbon in the northeast Atlantic in 2000–2001. *Journal of Geophysical Research: Oceans*, *110*(C10). https://doi.org/10.1029/2004JC002731

Sprintall, J., & Tomczak, M. (1993). On the formation of Central Water and thermocline ventilation in the southern hemisphere. Deep Sea Research Part I: Oceanographic Research Papers, 40(4), 827-848. https://doi.org/10.1016/0967-0637(93)90074-D

Stedmon, C. A., Markager, S., & Bro, R. (2003). Tracing dissolved organic matter in aquatic environments using a new approach to fluorescence spectroscopy. *Marine chemistry*, *82*(3-4), 239-254. https://doi.org/10.1016/S0304-4203(03)00072-0

Stott, D. E., & Martin, J. P. (1990). Synthesis and degradation of natural and synthetic humic material in soils. *Humic substances in soil and crop sciences: Selected readings*, 37-63. https://doi.org/10.2136/1990.humicsubstances.c3

Sukekava, C., Downes, J., Slagter, H. A., Gerringa, L. J., & Laglera, L. M. (2018). Determination of the contribution of humic substances to iron complexation in seawater by catalytic cathodic stripping voltammetry. *Talanta*, *189*, 359-364. https://doi.org/10.1016/j.talanta.2018.07.021

Swan, C. M., Siegel, D. A., Nelson, N. B., Carlson, C. A., & Nasir, E. (2009). Biogeochemical and hydrographic controls on chromophoric dissolved organic matter distribution in the Pacific Ocean. *Deep Sea Research Part I: Oceanographic Research Papers*, *56*(12), 2175-2192. https://doi.org/10.1016/j.dsr.2009.09.002

Tedetti, M., Cuet, P., Guigue, C., & Goutx, M. (2011). Characterization of dissolved organic matter in a coral reef ecosystem subjected to anthropogenic pressures (La Réunion Island, Indian Ocean) using multi-dimensional fluorescence spectroscopy. *Science of the total environment*, *409*(11), 2198-2210. https://doi.org/10.1016/j.scitotenv.2011.01.058

Tomczak, M., & Godfrey, J. S. (2003). *Regional oceanography: an introduction*. Daya books. https://doi.org/10.1016/C2009-0-14825-0

van den Berg, C. M. (1995). Evidence for organic complexation of iron in seawater. *Marine Chemistry*, *50*(1-4), 139-157. https://doi.org/10.1016/0304-4203(95)00032-M

Villa-Alfageme, M., Chamizo, E., Kenna, T. C., López-Lora, M., Casacuberta, N., Chang, C., ... & Christl, M. (2019). Distribution of 236U in the US GEOTRACES Eastern Pacific Zonal Transect and its use as a water mass tracer. *Chemical Geology*, *517*, 44-57. https://doi.org/10.1016/j.chemgeo.2019.04.003

Wagener, T., Metzl, N., Caffin, M., Fin, J., Helias Nunige, S., Lefevre, D., ... & Moutin, T. (2018). Carbonate system distribution, anthropogenic carbon and acidification in the western tropical South Pacific (OUTPACE 2015 transect). *Biogeosciences*, *15*(16), 5221-5236. https://doi.org/10.5194/bg-15-5221-2018

Wagner, S., Jaffé, R., & Stubbins, A. (2018). Dissolved black carbon in aquatic ecosystems. *Limnology and Oceanography Letters*, *3*(3), 168-185. https://doi.org/10.1002/lol2.10076

Weiss, R. F. (1970). The solubility of nitrogen, oxygen and argon in water and seawater. In *Deep Sea Research and Oceanographic Abstracts* (Vol. 17, No. 4, pp. 721-735). Elsevier. https://doi.org/10.1016/0011-7471(70)90037-9

Whitby, H., Bressac, M., Sarthou, G., Ellwood, M. J., Guieu, C., & Boyd, P. W. (2020a). Contribution of electroactive humic substances to the iron-binding ligands released during microbial remineralization of sinking particles. *Geophysical Research Letters*, *47*(7). https://doi.org/10.1029/2019GL086685

Whitby, H., Planquette, H., Cassar, N., Bucciarelli, E., Osburn, C. L., Janssen, D. J., ... & Sarthou, G. (2020b). A call for refining the role of humic-like substances in the oceanic iron cycle. *Scientific reports*, *10*(1), 1-12. https://doi.org/10.1038/s41598-020-62266-7

Wyrtki, K. (1967). Equatorial Pacific Ocean 1. *Int. J. Oceanol. & Limnol. Vol*, *1*(2), 117-147.

Whitby, H., & van den Berg, C. M. (2015). Evidence for copper-binding humic substances in seawater. *Marine Chemistry*, *173*, 282-290. https://doi.org/10.1016/j.marchem.2014.09.011

Wu, J., & Luther III, G. W. (1995). Complexation of Fe (III) by natural organic ligands in the Northwest Atlantic Ocean by a competitive ligand equilibration method and a kinetic approach. *Marine Chemistry*, *50*(1-4), 159-177. https://doi.org/10.1016/0304-4203(95)00033-N

Wünsch, U. J., Bro, R., Stedmon, C. A., Wenig, P., & Murphy, K. R. (2019). Emerging patterns in the global distribution of dissolved organic matter fluorescence. *Analytical Methods*, *11*(7), 888-893. https://doi.org/10.1039/C8AY02422G

Yamashita, Y., Cory, R. M., Nishioka, J., Kuma, K., Tanoue, E., & Jaffé, R. (2010). Fluorescence characteristics of dissolved organic matter in the deep waters of the Okhotsk Sea and the northwestern North Pacific Ocean. *Deep Sea Research Part II: Topical Studies in Oceanography*, *57*(16), 1478-1485. https://doi.org/10.1016/j.dsr2.2010.02.016

Yamashita, Y., & Tanoue, E. (2004). In situ production of chromophoric dissolved organic matter in coastal environments. *Geophysical Research Letters*, *31*(14). https://doi.org/10.1029/2004GL019734

Yamashita, Y., & Jaffé, R. (2008). Characterizing the interactions between trace metals and dissolved organic matter using excitationemission matrix and parallel factor analysis. Environmental Science & Technology,42(19), 7374–7379. https://doi.org/10.1021/es801357h

Yamashita, Y., & Tanoue, E. (2008). Production of bio-refractory fluorescent dissolved organic matter in the ocean interior. *Nature Geoscience*, *1*(9), 579-582. https://doi.org/10.1038/ngeo279

Yamashita, Y., & Tanoue, E. (2009). Basin scale distribution of chromophoric dissolved organic matter in the Pacific Ocean. *Limnology and Oceanography*, *54*(2), 598-609. https://doi.org/10.4319/lo.2009.54.2.0598

Zark, M., Christoffers, J., & Dittmar, T. (2017). Molecular properties of deep-sea dissolved organic matter are predictable by the central limit theorem: evidence from tandem FT-ICR-MS. *Marine Chemistry*, *191*, 9-15. https://doi.org/10.1016/j.marchem.2017.02.005

Zhao, S., Xue, S., Zhang, J., Zhang, Z., & Sun, J. (2020). Dissolved organic matter-mediated photodegradation of anthracene and pyrene in water. *Scientific Reports*, *10*(1), 1-9. https://doi.org/10.1038/s41598-020-60326-6

Zheng, Q., Chen, Q., Cai, R., He, C., Guo, W., Wang, Y., ... & Jiao, N. (2019). Molecular characteristics of microbially mediated transformations of Synechococcus-derived dissolved organic matter as revealed by incubation experiments. *Environmental microbiology*, *21*(7), 2533-2543. https://doi.org/10.1111/1462-2920.14646

Zigah, P. K., McNichol, A. P., Xu, L., Johnson, C., Santinelli, C., Karl, D. M., & Repeta, D. J. (2017). Allochthonous sources and dynamic cycling of ocean dissolved organic carbon revealed by carbon isotopes. *Geophysical Research Letters*, *44*(5), 2407-2415. https://doi.org/10.1002/2016GL071348

Ziolkowski, L. A., & Druffel, E. R. (2010). Aged black carbon identified in marine dissolved organic carbon. *Geophysical Research Letters*, *37*(16). https://doi.org/10.1029/2010GL043963

Zsolnay, Á. (2003). Dissolved organic matter: artefacts, definitions, and functions. *Geoderma*, *113*(3-4), 187-209. https://doi.org/10.1016/S0016-7061(02)00361-0

Zsolnay, A., Baigar, E., Jimenez, M., Steinweg, B., & Saccomandi, F. (1999). Differentiating with fluorescence spectroscopy the sources of dissolved organic matter in soils subjected to drying. Chemosphere, 38(1), 45-50. https://doi.org/10.1016/S0045-6535(98)00166-0

Supplementary material

Table S1. Limits of detection (LOD) for the different detectors coupled to SEC in a seawater matrix (Bay of Brest, S = 35 psu). Injection volumes were 2 mL. LOD were calculated according to the IUPAC recommendation (1978): LOD = 3 × SE where « SE » is the mean standard error (or standard error) of the blanks over 10 consecutive measurements of a coastal water of the Bay of Brest, previously irradiated (3h) with UV light (Dulaquais et al., 2018b). The expected contents in each fraction operationally defined by SEC are those proposed by Huber et al. (2011) and in this study.

Organic carbon					(µMC)		
Fraction		DOC	BP	HS	BB	LMW acids	LMW neutrals
Expected content	Huber et al. (2011)		Proteinic matter Polysaccharides	Humic matter including Fulvic and humic acids	HS-like material of LMW	Anions at the pH of the buffer (~ 7)	Hydrophilic/ amphiphilic compounds of low ion density
	This study				Degradation by-products of BP	Small and degradated HS	
LOD		2.3	0.4	0.2	0.1	1.0	3.0

	Organic nitrogen (µMN)		Aromatic carbon (%)	
Fraction	BP	HS	BP	HS
LOD	0.2	0.2	0.6	0.1

Table S2. Analyses performed on DOM for each different cruise presented in this study. TOC-V analyses during CLIVAR (*) were carried out by Swan et al. (2009).

	Analytical method			
Cruise – Station – Coordinates	**SEC**	**TOC-V**	**Fluorescence**	**CSV (eHs)**
TONGA – **St. 8** – 20° 24.431'S, 166° 35.675'W	✓	✓	✓	✓
US-GP15 – **St. 39** – 19° 59.99'S, 152° 00.01'W	✓			
CLIVAR P16 – **St.9** – 20°S; 150°W		✓*		

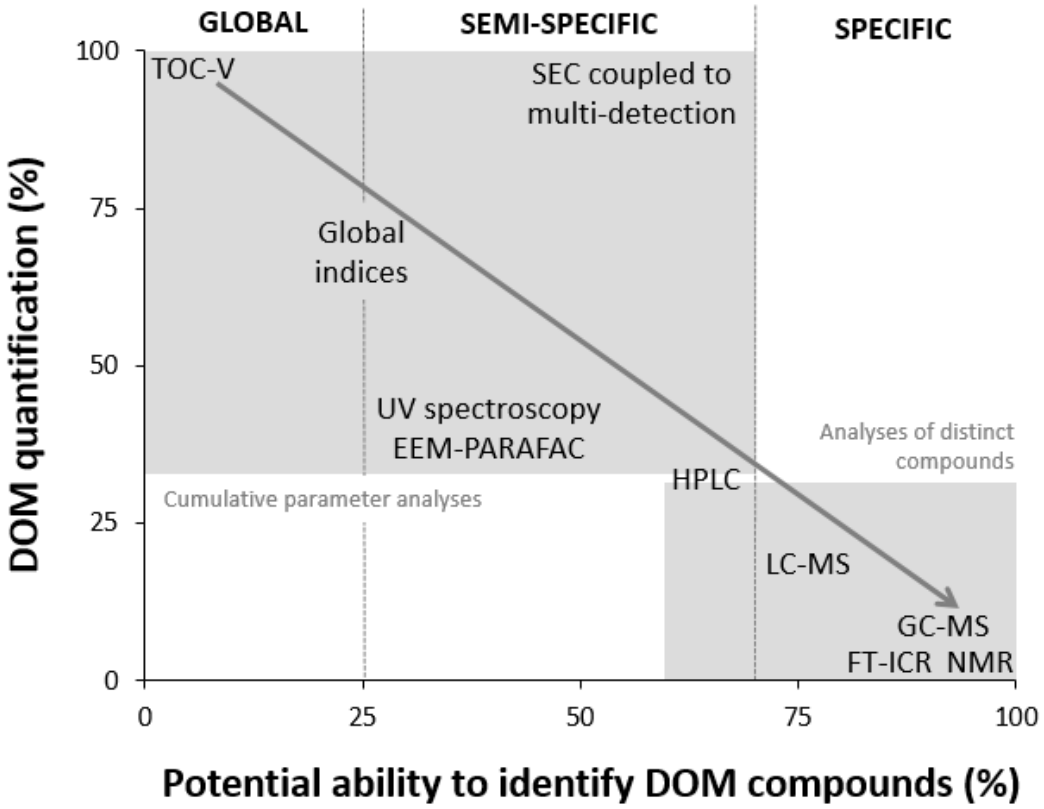

Figure S1. Analytical window of the different approaches applied to DOM analysis. TOC = Total Organic Carbon; SEC: Size Exclusion Chromatography; EEM-PARAFAC: Excitation Emission fluorescence Matrice-Parallel Factor Analysis; HPLC: High Performance Liquid Chromatography; LC-MS: Liquid Chromatography-Mass Spectrometry; GC-MS: Gas Chromatography-Mass Spectrometry; FT-ICR: Fourier Transform Ion Cyclotron Resonance; NMR: Nuclear Magnetic Resonance. Figure based on http://doc-labor.de/?page_id=13.

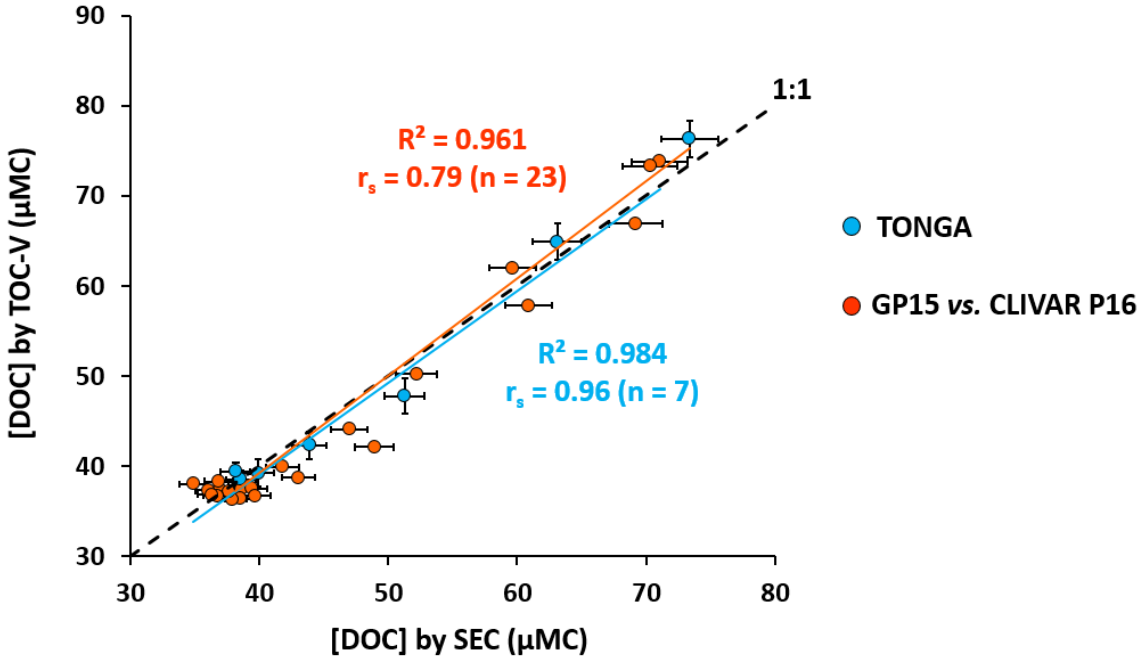

Figure S2. Comparisons between the datasets from GP15 St. 39 (19° 59.99'S, 152° 00.01'W) by SEC and historical data from CLIVAR P16 St. 9 (20°S; 150°W) by TOC-V, as well as the two TONGA datasets (SEC and TOC-V) at St. 8 (20° 24.431'S, 166° 35.675'W). Spearman coefficient r_s close to 1 in both cases indicates the strong correlation between DOC concentrations determined by TOC-V and SEC.

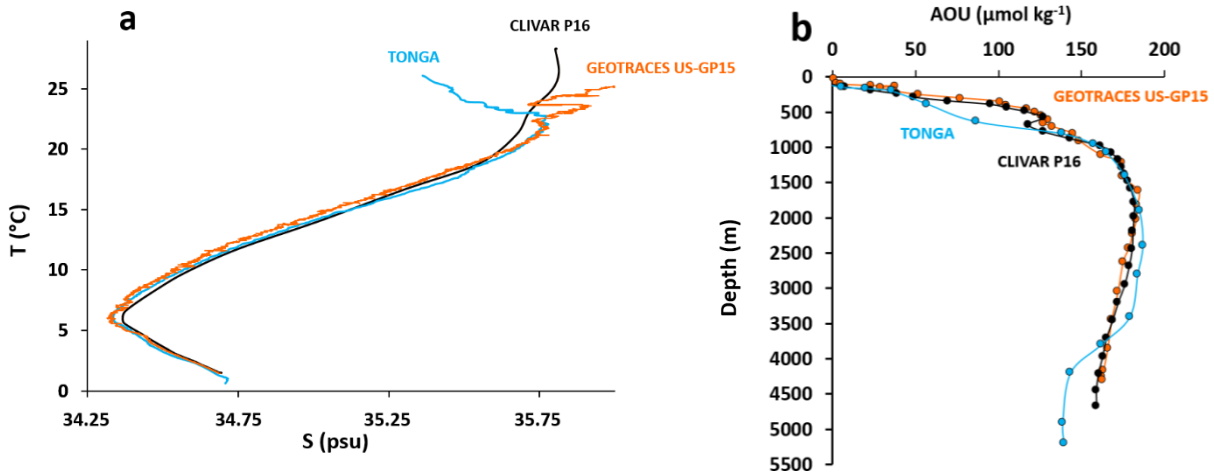

Figure S3. (a) Intercomparison of the temperature/salinityAU diagram between TONGA St. 8 (20° 24.431'S, 166° 35.675'W), GEOTRACES US-GP15 St. 39 (19° 59.99'S, 152° 00.01'W) and CLIVAR P16 St. 9 (20°S; 150°W). **(b)** Intercomparison between vertical profiles of apparent oxygen utilization (AOU) for TONGA, GEOTRACES and CLIVAR P16 (same stations).

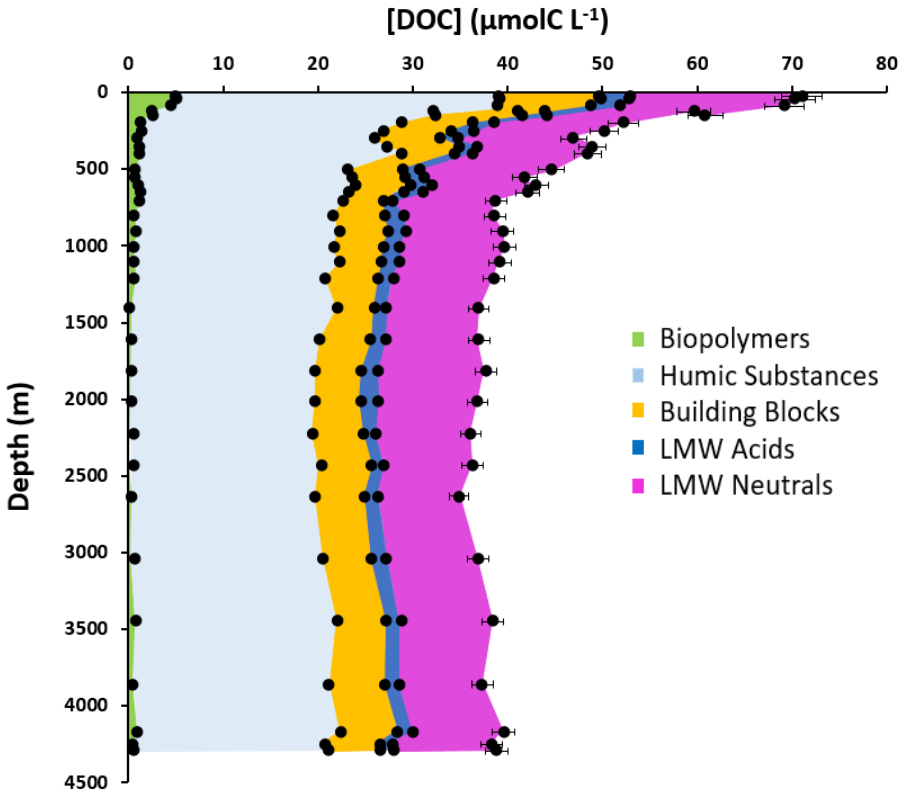

Figure S4. Vertical profiles of the DOC concentrations (µMC) in the five operational fractions defined by SEC, along the water column at 19° 59.99'S, 152° 00.01'W during the GEOTRACES US-GP15 expedition. Non-visible error bars are covered by the symbols.

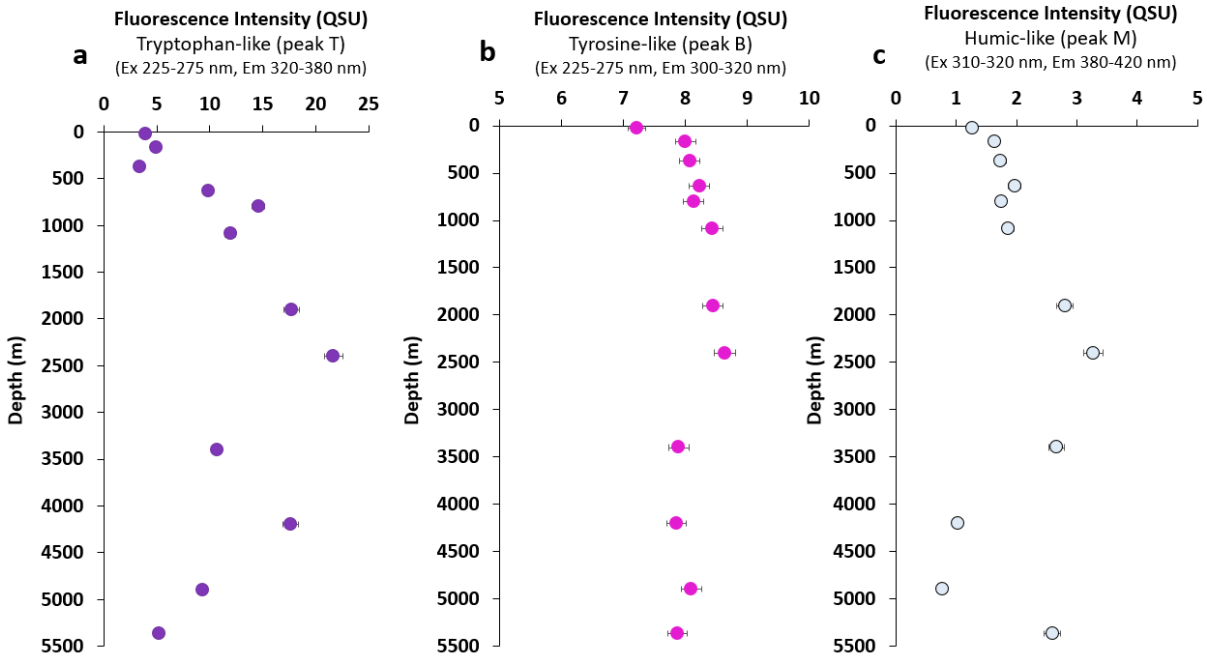

Figure S5. Vertical profiles of **(a)** tryptophan-like fluorescence intensity (T); **(b)** tyrosine-like fluorescence intensity (B); **(c)** marine humic-like fluorescence intensity (M); according to the nomenclature defined by Coble (1996).